

1-1-2014

Accumulation Of Subcortical Iron As A Modifier Of Volumetric And Cognitive Decline In Healthy Aging: Two Longitudinal Studies

Ana Marie Daugherty
Wayne State University,

Follow this and additional works at: http://digitalcommons.wayne.edu/oa_dissertations



Part of the [Cognitive Psychology Commons](#), and the [Neurosciences Commons](#)

Recommended Citation

Daugherty, Ana Marie, "Accumulation Of Subcortical Iron As A Modifier Of Volumetric And Cognitive Decline In Healthy Aging: Two Longitudinal Studies" (2014). *Wayne State University Dissertations*. Paper 964.

This Open Access Dissertation is brought to you for free and open access by DigitalCommons@WayneState. It has been accepted for inclusion in Wayne State University Dissertations by an authorized administrator of DigitalCommons@WayneState.

**ACCUMULATION OF SUBCORTICAL IRON AS A MODIFIER OF VOLUMETRIC
AND COGNITIVE DECLINE IN HEALTHY AGING: TWO LONGITUDINAL
STUDIES**

by

ANA M. DAUGHERTY

DISSERTATION

Submitted to the Graduate School

of Wayne State University,

Detroit, Michigan

in partial fulfillment of the requirements

for the degree of

DOCTOR OF PHILOSOPHY

2014

MAJOR: PSYCHOLOGY

Approved by:

Advisor

Date

ACKNOWLEDGMENTS

This work was supported in part by grant 1893.SAP from the Blue Cross Blue Shield of Michigan Foundation student awards program, Rumble research fellowship from the Wayne State University Graduate School, and pre-doctoral training fellowship from the Institute of Gerontology at Wayne State University to AMD; and National Institute on Aging grant R37-AG011230 to NR. Many thanks to my dissertation committee: Drs. Naftali Raz, Noa Ofen, Jessica Damoiseaux, and E. Mark Haacke. Finally, Drs. Cheryl Dahle, Andrew Bender, Yiqin Yang, Karen Rodrigue and Kristen Kennedy, and colleague Peng Yuan contributed to the longitudinal data collection and method development.

TABLE OF CONTENTS

Acknowledgments	ii
List of Tables	iii
List of Figures	iv
Chapter I – Introduction	1
Chapter II – Research Design	12
Chapter III – General Methods	17
Chapter IV – Results	31
Chapter V – Discussion	44
Appendix A: Longitudinal sample attrition	53
Appendix B: Manual tracing methods	54
Appendix C: Longitudinal latent model construction	56
References	64
Abstract	82
Autobiographical Statement	84

LIST OF TABLES

Table 1: Demographic profile of Sample 1	17
Table 2: Demographic profile of Sample 2	17
Table 3: Latent constructs and measures for identification in analyses	30
Table 4: Two-year mean change and variance in change in regional iron and volume	32
Table 5: Seven-year mean change and variance in change in regional iron and volume ...	33
Table A1: Sample 1 longitudinal attrition	54
Table A2: Sample 2 longitudinal attrition	54

LIST OF FIGURES

Figure 1: A sketch of study aims and hypothesized relationships between age and the target variables	2
Figure 2: Aberrations in iron metabolism in an aging neuron	5
Figure 3: Example manual tracing on 4 T and 1.5 T images	21
Figure 4: Comparison of manually obtained T2* values (baseline 4T data) compared to reports of post-mortem values	22
Figure 5: An over-head diagram of the test vMWM environment	26
Figure 6: Sample 1 regional average T2* at baseline and at 2-year follow-up	31
Figure 7: Individual two-year change trajectories in striatal volume and iron	35
Figure 8: Individual seven-year change trajectories in globus pallidus volume and iron	37
Figure 9: Individual seven-year change trajectories in putamen volume and iron	37
Figure 10: Simplified parallel process latent change score models of caudate and hippocampal iron and volume effects on verbal working memory	40
Figure 11: Simplified parallel process latent change score model of caudate iron and volume effects on spatial navigation efficiency	43

CHAPTER I

INTRODUCTION

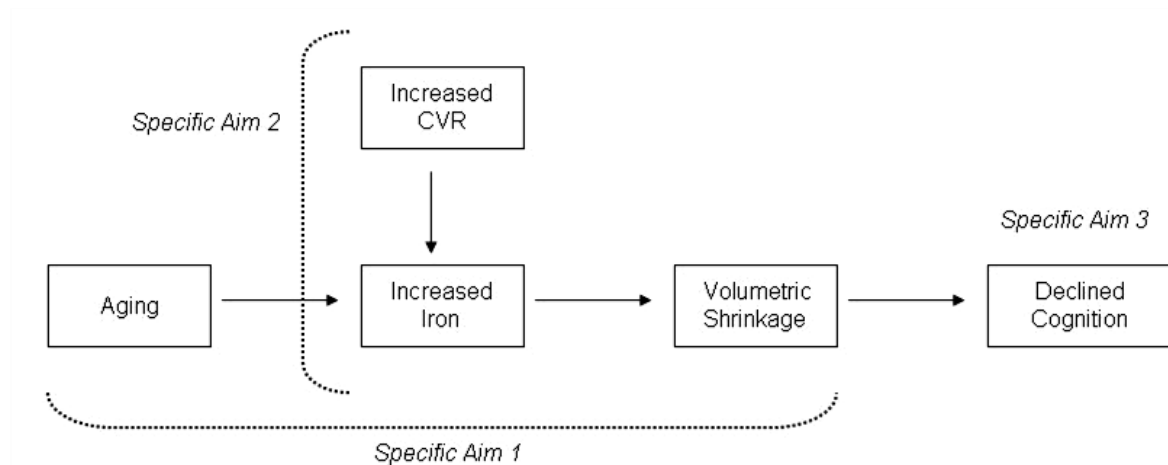
Declines in regional brain volume (Raz and Kennedy, 2009) and decreased cognitive function (Horn and Donaldson, 1980) are hallmarks of normal aging. However, age-related differences are not uniform. Patterns of decline vary between brain regions (Raz et al., 2010) as well as affected cognitive functions (Horn and Donaldson, 1980; Lindenberger et al., 1993; Park, 2000). Further, there are individual differences in the magnitude of decline across the lifespan (Raz, 2005; Raz and Kennedy, 2009). The lack of uniformity in brain aging suggests additional mediating factors that modify regional and individual aging trajectories (Raz et al., 2004; Raz, 2005; Raz and Kennedy, 2009). The modifying factors are manifold and likely interact.

Compromised neuronal metabolism by cellular factors or systemic cardiovascular health may differentiate age-sensitive neural and cognitive systems. Accumulation of non-heme iron in the brain is one such cellular factor that disrupts metabolism via oxidative stress (Harman, 1956; see Mills et al., 2010 and Bartzokis, 2011 for reviews). However, deleterious effects of iron in healthy brain aging are poorly understood, and even less is known of their cognitive consequences and interactions with cardiovascular health. This uncertainty about true cumulative effect of brain iron in healthy aging largely stems from the fact that change has been inferred from cross-sectional studies that are incapable of estimating individual differences in change and evaluating their mediators (Maxwell and Cole, 2007; Lindenberger et al., 2011; Raz and Lindenberger, 2011). In the first *in vivo* longitudinal study of brain iron, Walsh and colleagues (2014) recently reported increase in subcortical iron content, but did not examine individual differences or the influence of confounding age-related risk factors. A need of addressing these issues served as the main impetus for the series of studies presented here.

Although interventions are not included in the present study, longitudinal assessment of iron content in healthy aging brains may identify an early marker of later-life decline with possible treatment (see Schenck and Zimmerman, 2004). Determination of injurious metabolic factors will inform lifetime strategies to promote successful aging.

The present study is a longitudinal assessment of changes in and mutual influences of regional iron content, regional brain volumes, systemic cardiovascular health, and cognitive performance. The aims of this study are threefold. The first aim is to determine the longitudinal change and, more importantly, variance in change of iron content across brain regions, and to elucidate the relationship between iron content and regional brain shrinkage in healthy aging. Second, I sought to investigate the role of sub-clinical increase in cardiovascular risk in age-related iron accumulation and volumetric decline. The final aim was to evaluate the indirect effects of aging on two age-sensitive cognitive domains—working memory and spatial navigation—mediated by regional changes in volume and iron content.

Figure 1. A sketch of study aims and hypothesized relationships between age and the target variables.



1.1 Iron as an Oxidative Stress Factor in Brain Aging

In biological systems, iron exists in two forms: heme and non-heme iron. Heme iron is in

the core of the hemoglobin molecule and is thus present in the brain wherever blood flows or accumulates (Tingey, 1938). Heme iron in circulating cerebral blood has no known deleterious effects and is therefore not considered to contribute to neurodegeneration (Halliwell, 1992; Mills et al., 2010). However, other sources of heme iron (i.e., cerebral microbleed or hemosedrin) are less benign (see Loitfelder, Seiler, Schwingenschuh, and Schmidt, 2011 for a review). Whereas the prevalence of cerebral microbleeds in healthy adults is relatively low (Yates et al., 2011; see Loitfelder, Seiler, Schwingenschuh, and Schmidt, 2011 for a review), subcortical non-heme iron appears to continuously accumulate across the lifespan (Daugherty and Raz, 2013). In contrast to its heme form, excess free non-heme iron has been consistently identified as a correlate of neurological pathology (see Bartzokis, 2011; Zecca et al., 2004; Lauffer, 1992 for reviews) and may be a harbinger of impairment.

Intracellular non-heme iron is a critical oxidizing agent in normal metabolism, but in excess promotes oxidative stress and thus is a potential factor in cellular deterioration (see Mills et al., 2010 for a review). Healthy neurons store non-heme iron for lipid peroxidation, mitochondrial ATP generation, and DNA replication (see Mills et al., 2010 for a review). Oligodendrocytes depend on bioavailability of iron for myelination, the precise mechanism of which is unclear, but is likely due to iron as a cofactor necessary for energy production (Todorich et al., 2009). However, iron-catalyzed reactions commonly produce reactive oxygen species (OH^\cdot ; hydroxyl anions) that cause oxidative stress. Thereby an excess of unregulated soluble non-heme iron can become toxic (see Zecca et al., 2004; Mills et al., 2010 for reviews). Cellular non-heme iron is normally bound to transferrin (Bloch et al., 1985; Lauffer, 1992) or sequestered in ferritin (Diezel, 1955; Fisher et al., 2006), which appears to control the potential deleterious effects. In a healthy neuron, upwards of 90% of non-heme iron is sequestered in

ferritin (Jara et al., 2006), where it remains until mitochondria signal solubilization for immediate metabolism (Chrichton and Ward, 1992).

Intracellular non-heme iron concentration depends on metabolic need (see Mills et al., 2010 for a review). Outside of ferritin sequestration, metabolically necessary soluble non-heme iron (mostly Fe^{2+}) is represented as the labile pool (approximately 1 μM) that is bound to amino acids (Lauffer, 1992), ATP (Cabantchik et al., 2002) and metallochaperones (Mills et al., 2010). During metabolism, neurons express a unique combination of transport proteins that strictly regulate soluble non-heme iron (Dong et al., 2008; Gunshin et al., 1997; Moos et al., 2007; see Mills et al., 2010 for a review). The transport proteins bind and ferry non-heme iron from ferritin sequestration and in the labile pool until the iron is required, neutralizing the iron and thereby limiting the rate of oxidative stress (Dong et al., 2008; Gunshin et al., 1997; Moos et al., 2007; see Mills et al., 2010 for a review). The delicate intracellular equilibrium depends upon sufficient concentrations of soluble non-heme iron to support normal metabolism and effective management of non-heme iron by binding proteins to minimize oxidative stress (see Hare et al., 2013 for a review).

In an unbound state, accumulated non-heme iron is free to aggressively react within the cytosol and thus promotes oxidative stress (see Zecca et al., 2004; Moos and Morgan, 2004; Mills et al., 2010; Hare et al., 2013 for reviews). Recent evidence suggests that cellular increase in non-heme iron follows aberrant transport and storage mechanisms (Singh et al., 2009; Zhang et al., 2009; Bartzokis et al., 2010), which become insufficient to manage the toxic concentrations. The failure of iron concentration control has been linked to multiple factors, including aberrations of dopamine and serotonin metabolism (Berg et al., 2007), mutations in mitochondrial and nuclear DNA (Hamilton et al., 2001), inflammation and accelerated apoptosis

(Zhang et al., 2009), and abnormal mitochondrial function (Mallikarjun et al., 2014). (See Figure 2 for an illustration of aberrant iron metabolism in neuronal aging.) These microstructural changes have been hypothesized to affect the progressive global declines in aging (see Raz, 2005 for a review); however, the cause of these changes is uncertain. It is plausible that the accumulation of non-heme iron is both a cause and an effect of increased production of reactive oxygen species and the ensuing oxidative stress (see Cherubini et al., 2009).

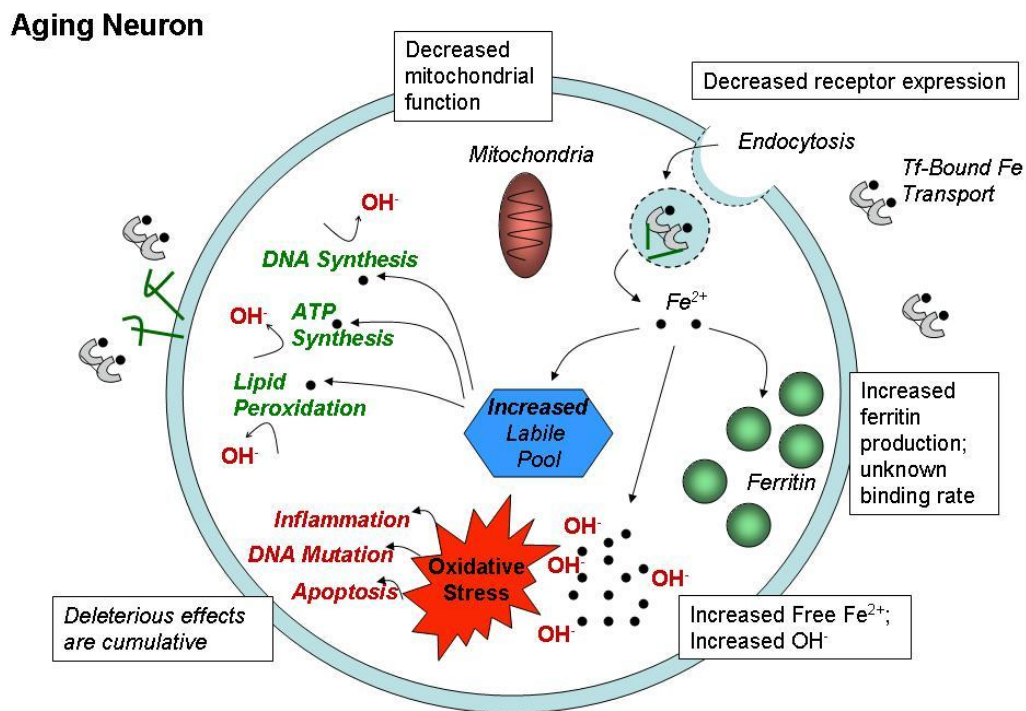


Figure 2. Aberrations of iron metabolism that precipitates oxidative stress and neuronal dysfunction in aging. The figure is constructed from evidence reviewed in Mills et al., 2010; Zecca et al., 2004; and Chrichton and Ward, 1992.

1.2 Iron Promotes Regional Atrophy in Aging

Cellular damage associated with non-heme iron accumulation may explain many of the cumulative structural changes observed in aging and neurodegenerative disease (Hallervorden

and Spatz, 1922; Harman, 1956; Bartzokis et al., 1994, 1997, 1999). Several studies have noted high concentrations of iron in Alzheimer's disease co-localized with tangles (House et al., 2004), plaques (Quintana et al., 2006) and amyloid burden (Rival et al., 2009). Some have hypothesized that oxidative stress from toxic concentrations of free iron is a primary cause of demyelination in normal aging and exacerbation of such in Alzheimer's disease (Bartzokis, 2011). In healthy aging, iron concentration in brain tissue is regionally specific and the magnitude of age differences therein vary across the affected regions (Drayer, 1988).

Subcortical regions have higher concentrations of non-heme iron relative to subcortical white matter and the cerebral cortex. The basal ganglia have particularly large concentrations of iron, which are relatively low in childhood and early adulthood but appear to increase in the brains of middle-aged and older adults (Hallgren and Sourander, 1956; Thomas et al., 1993; Bartzokis et al., 1994; Martin, Ye, and Allen, 1998; Harder et al., 2008; Siemonsen et al., 2008; Xu et al., 2008; Aquino et al., 2009; Pfefferbaum et al., 2009, 2010; Haacke et al., 2010; Bilgic et al., 2011; Kumar et al., 2011). A recent meta-analysis of cross-sectional magnetic resonance imaging (MRI) studies identified age-related differences in iron content within the basal ganglia, with the globus pallidus evidencing modestly higher content in older brains and striatum showing a larger age-related increase (Daugherty and Raz, 2013). The accumulation of iron in the caudate and putamen may explain to some extent their significantly smaller volumes in advanced age (volumetric correlation with age $r = -0.30$ and -0.43 , respectively; Raz, 2004), and longitudinal change as well as significant individual differences therein (Raz et al., 2005; Raz et al., 2010). Similarly, age differences in hippocampal volume (Raz et al., 2004, 2005, 2010) may be associated with moderate increase in iron content (Rodrigue, Daugherty, Haacke, Raz, 2013). For the lack of longitudinal investigations, these conjectures remain untested.

Absent of disease, non-linear lifespan increases in particular brain regions may reflect early-life concentrations, as the basal ganglia have persistently larger concentrations throughout development compared to the rest of the brain (Thomas et al., 1993). A single longitudinal study supports an increase in striatal iron in healthy adults within two years (Walsh et al., 2014). However, it did not adequately account for the possible relationship between early life values and later accumulation. Amongst other limitations, this study was in a small sample and was a simple effects analysis of change in iron only. Therefore, additional longitudinal study is warranted to understand the change in brain iron in the context of change in other neural and health correlates of age.

1.3 Cardiovascular Risk Factors Exacerbate the Increase in Iron Content and Structural Shrinkage

Non-linear patterns of specific regional changes across the adult lifespan and individual differences therein (Raz et al., 2004, 2005; Raz, 2005) suggest potential mediating factors between neural and cognitive systems. The cluster of common cardiovascular risk factors (i.e., hypertension or high-normal blood pressure, elevated blood glucose and triglycerides, and decreased high-density lipoprotein) has been termed metabolic syndrome (Grundy et al., 2005). Metabolic syndrome (MetS) increases the risk for a cardiovascular event and even subclinical elevation in these factors exacerbates neural and cognitive differences in aging to partially explain individual differences (Dahle, Jacobs, Raz, 2009; Head et al., 2002; Raz et al., 2005). Symptoms of MetS are also associated with greater regional iron content (Jehn, Clark, and Guallar, 2004; Fernandez-Real, Lopez-Bernejo, and Ricart, 2005; Ascherio et al., 1994; Alissa et al., 2007; Raz, Rodrigue, and Haacke, 2007) and oxidative stress (Berry et al., 2001). Further, increased brain iron is observed in patients with cerebrovascular disease (Hirai et al., 1996) and

diabetes (Rajpathak et al., 2009; Shi et al., 2006).

The links between brain iron content and MetS are unclear and likely reflect multiple phenomena. For instance, iron may contribute to MetS through the promotion of inflammation via oxidative stress. Indeed, greater concentrations of non-heme iron increase inflammation (Joseph et al., 2005) and accelerate apoptosis (Zecca et al., 2004; Zhang et al., 2009). However, it is unclear if increased iron is a cause of MetS, or if concentrations are effected by elevations in cardiovascular risk factors. Iron is systemically delivered via vascular supply (Mills et al., 2010) and it is plausible that regional differences in iron concentration are due to differential sensitivity to risk factors. Non-heme iron concentrations may interact with other metabolic factors similarly delivered, including oxygen (Mills et al., 2010; Raz, 2005) that is necessary in the production of free radicals that promote oxidative stress. Thus, individual differences in cardiovascular risk factors may account for differential regional changes in iron concentration and subsequent volumetric shrinkage. Due to the lack of longitudinal studies, the mutual effects of cardiovascular health and brain iron in healthy human aging remain confounded. Therefore, it is unknown whether disruption of cellular iron homeostasis underlies age-related cognitive changes on its own or via regional brain shrinkage (see Mills et al., 2010 and Bartzokis, 2011 for reviews).

1.4 Interaction of Iron Concentration, Regional Shrinkage and Cardiovascular Health to Explain Cognitive Decline

Iron accumulation with age may cause cognitive declines through structural or functional (e.g., altered neurotransmission) damage that can be traced to oxidative stress. This potential relationship with cognitive function is poorly understood for the lack of study in healthy human aging. In the extant cross-sectional studies in healthy adults, increased iron content in

subcortical structures was associated with poorer memory performance (Bartzokis et al., 2011; Rodrigue, Haacke, and Raz, 2011; Rodrigue, Daugherty, Haacke, and Raz, 2012) and slow motor response (Pujol et al., 1992). Elevated concentrations of brain iron have also been correlated with cognitive deficits in Alzheimer's disease (Qin et al., 2011; Ding et al., 2009), dementia (Rombouts et al., 2007) and multiple sclerosis (Brass et al., 2006). In a healthy lifespan sample, increased iron content in the basal ganglia (but not hippocampus) was associated with poorer spatial navigation skills, and partly explained age-related deficits therein (Daugherty, master's thesis). In another lifespan sample, increased hippocampal iron correlated with smaller hippocampal volumes, and both factors explained poorer memory function with age (Rodrigue, Daugherty, Haacke, and Raz, 2012). However, in these healthy lifespan samples, subclinical variation in MetS factors did not account for individual variability in regional iron concentration or volume (Daugherty, master's thesis; Rodrigue, Daugherty, Haacke, and Raz, 2012).

Cross-sectional comparisons may minimize individual differences in cardiovascular health and underestimate consequent effects in regional volumetry and cognitive function. Cross-sectional studies are inherently incapable of providing valid estimates of individual differences in change (Maxwell and Cole, 2007; Lindenberger et al., 2011; Raz and Lindenberger, 2011). Longitudinal study is necessary to identify the role of iron in human neural and cognitive aging. If age-related decline depends upon the accumulation of non-heme iron, then individual differences in this factor should account for the individual differences in longitudinal decline trajectory (see Underwood, 1975). Therefore, the present study will estimate regional iron content and volume *in vivo* within two independent, healthy adult samples with concurrent longitudinal measurements of cardiovascular health and cognitive function.

1.5 Review of in vivo Iron Estimation: T2 Relaxometry*

Evaluation of the effects of iron on age-related changes in brain and cognition depends on *in vivo* estimates of brain iron content, and MRI is well suited to obtain such measures. When exposed to a magnetic field, the magnetic particles in the brain are excited and the phase of their precession changes in proportion to their unique susceptibility. MRI methods of iron estimation measure the time required for the transverse excitation to dissipate and the particles to recover their pre-excitation phase. The addition of the susceptibility component ($R2'$) to the transverse relaxation rate ($R2$) produces a more general relaxation rate index, $R2^*$, with $R2^*=R2+R2'$. The inverse index, $T2^*=1/R2^*$ is frequently used to describe the total transverse relaxation process, and short $T2^*$ relaxation times are proportional to larger iron concentrations (Thomas et al., 1993). On $T2^*$ -weighted images, iron-rich regions appear dark and differences in iron content can be measured by relative differences in image intensity values.

Although $T2^*$ offers a robust *in vivo* measure of brain iron, it is not without limitations. The primary confound of $T2^*$ is the contribution of myelin to transverse relaxation time (Fukunaga et al., 2010; Langkammer et al., 2012; Lodygensky et al., 2012) that can be misinterpreted as a difference in iron content. Thus, in deep white matter regions and areas with myelinated fibers, $T2^*$ estimates lack specificity (see Hasan et al., 2008, 2009). Field-dependent rate increase (FDRI), another MRI method of iron measurement, is deemed independent of this bias (Bartzokis et al., 2007). In a recent meta-analysis, age-related differences in the basal ganglia estimated from $T2^*$ agreed highly with FDRI-based estimates (Daugherty and Raz, 2013). Thus, $T2^*$ may be negligibly influenced by the small myelinated fibers in the striatum (Xiang et al., 2005) and can be considered a valid estimate of iron content in subcortical structures. Although age differences in $T2^*$ may be further confounded by comorbid calcification that affects the index in the same manner as iron does (Naderi et al., 1993).

However, the influence of calcium deposits can be separately estimated only with phase imaging and the effect of calcium on T2* is probably small in healthy aging (Haacke et al., 2005).

A problematic aspect of T2*-based and other *in vivo* iron estimation methods is that these methods cannot readily distinguish between heme and non-heme iron sources. The pathological role of iron in aging appears specific to non-heme and not heme iron, which is present wherever cerebral blood flows (arteries and veins) or accumulates (i.e., cerebral bleed or hematoma). MRI relaxation times are affected by both sources of iron in a similar fashion. The transverse relaxation component of T2* (T2) correlates with regional cerebral blood volume (Anderson et al., 2005) and susceptibility-specific T2' decreases with age in relation to physiological changes in blood oxygenation and vascular health (Wagner et al., 2012). A meta-analysis of *in vivo* MRI studies suggests that although T2* encompasses the T2 relaxation component, estimates of age-differences in iron content derived from T2 and T2* within subcortical regions are equivalent (Daugherty and Raz, 2013). Thus the effect of cerebral blood volume on iron estimates in these structures may be negligible. To further reduce the likelihood of misinterpreting cerebral blood as non-heme iron, manual tracing on high-resolution images can exclude major vessels. Despite limitations (Gomori and Grossman, 1993; Schenck, 1995; Schenker et al., 1993; Vymazal et al., 1995a, 1995b), T2*-based *in vivo* measures of brain iron have been validated against post-mortem data and phantom measurements across several brain regions (Antonini et al., 1993; Bizzi et al., 1990; Peran et al., 2007, 2009; Pujol et al., 1992; Brass et al., 2006; Thomas et al., 1993; Bartzokis et al., 1994).

CHAPTER II

RESEARCH DESIGN

Specific Aim 1. Determine the change in iron content across brain regions and establish its association with regional shrinkage of brain tissue in healthy aging.

1.1 Rationale. Regional iron accumulation is suggested to influence volumetric shrinkage via oxidative stress and related apoptosis. Cross-sectional studies show larger brain iron concentrations in later life that differentiate across regions (Daugherty and Raz, 2013; Hallgren and Sourander, 1956). Structures that are vulnerable to large age-related volume reductions are also those shown to have high iron concentrations in later life. The basal ganglia have markedly high early-adulthood concentrations that appear to increase with age (Daugherty and Raz, 2013), and the caudate and putamen have demonstrably large volumetric differences in later life (Raz et al., 2005; 2010). The hippocampus also evidences increased iron content and volumetric decline across the lifespan (Rodrigue, Daugherty, Haacke, and Raz, 2012). Therefore, iron content and volume will be estimated *in vivo* within these regions of interest (ROIs).

As a control region, iron and volumes of the lamina quadrigemina will also be measured. The lamina quadrigemina are composed of the inferior (auditory pathway) and superior (visual pathway) colliculi and have not been studied in human aging. However, in rodents, equivalent nuclei have low iron concentrations (Hare et al., 2012; Hill and Switzer, 1984), and MRI measures of iron in the lamina quadrigemina in humans appear to be unrelated to age (Daugherty and Raz, unpublished data). Similarly, the regional volume is expected to remain stable with age, although there are no known studies.

1.2 Methods. A single rater (A.M.D.) manually demarcated ROIs across contiguous

slices informed by anatomical definitions. Manual demarcation is preferred over automated methods, as it will emphasize anatomical boundaries, allow manual exclusion of vascular objects, and reduce residual error. Further, due to image inhomogeneity and templates commonly based on young brains, automated sampling may reduce age-related variance. Therefore, the rater (A.M.D.) developed anatomically-informed rules and confirmed reliability with intra-class correlation coefficients (ICC(3); Shrout and Fleiss, 1979) exceeding 0.90. Average T2* relaxation time was estimated for right and left hemispheres separately in each ROI, with smaller values corresponding to larger iron content. Similarly, bilateral volumes of each ROI were calculated from the same manual demarcation.

These regional estimates were obtained in two independent samples of healthy adults. The first sample (N = 89, age 19-77 years at baseline) was assessed twice within approximately 2 years. In a latent change score model, change in regional volume and T2* were estimated with age, sex, and baseline volume and baseline T2* as covariates. Change in iron content (T2*) was postulated to precede volumetric change, and the directionality of the effects were tested with alternative model construction. These relationships were further tested using a latent growth curve model approach in a second lifespan sample (N = 32, age 50-76 years at baseline) that was assessed four times across 7 years.

Specific Aim 2. Investigate the role of metabolic syndrome indicators and pro-inflammatory biomarkers in age-related iron accumulation and volumetric decline.

2.1 Rationale. Poor cardiovascular health (i.e., MetS and inflammation) may cause increase in iron concentration and exacerbate consequent atrophy. MetS is associated with increased brain iron concentrations (Jehn, Clark, and Guallar, 2004; Fernandez-Real, Lopez-Bernejo, and Ricart, 2005; Ascherio et al., 1994; Alissa et al., 2007), with even greater increase

in cerebrovascular disease (Hirai et al., 1996) and diabetes (Rajpathak et al., 2009; Shi et al., 2006). Absent major pathology, subclinical elevation in these factors partially accounts for greater brain iron content in aging (Raz, Rodrigue, and Haacke, 2007) and is correlated with increased inflammation (Joseph et al., 2005; see Zecca et al., 2004 for a review). Increase in brain iron may follow directly from the factors subsumed under the rubric of decreased cardiovascular health, or indirectly in interaction with other metabolic indicators that are delivered via vascular supply along with iron.

Regional differences in iron content and subsequent volumetric shrinkage may be explained by differential sensitivity to cardiovascular risk factors. The basal ganglia (Feekes and Cassell, 2006) and hippocampus (Duvernoy, 1988) are highly vascularized and sensitive to perturbations of vascular supply and to hypoxia (Pulsinelli et al., 1982; Petito and Pulsinelli, 1984; Uehara, Tabuchi and Mori, 1999; Hawker and Lang, 1990); therefore, cardiovascular risk factors are hypothesized to exacerbate the age-related increase in iron within these regions. The lamina quadrigemina also have dense vascularization (Duvernoy, 1999) and these regions may also be vulnerable to cardiovascular risk; although total iron content is hypothesized to remain low even with subclinical increase in risk factors.

2.2 Methods. Metabolic syndrome score (MetS) was computed by combining the measures of fasting blood glucose, total triglycerides, high-density lipoprotein cholesterol, as well as diagnosed or observed hypertension. These cardiovascular risk indices are age-related and have been shown to interact with volume differences (Raz, Rodrigue, and Haacke, 2007; Raz et al., 2005). However, in our prior studies we found that subclinical elevations in these factors did not account for cross-sectional differences in iron content (Daugherty, master's thesis; Rodrigue, Daugherty, Haacke, and Raz, 2012).

Chronic inflammation is an additional cardiovascular risk factor and is postulated to account for declines in aging and neurodegenerative disease (Mattson and Shea, 2003). Chronic inflammation is suggested to directly influence iron concentration and apoptosis (Moos and Morgan, 2004) and may have a more specific effect on iron-related aging than the other systemic cardiovascular health factors. The present study included indices of chronic inflammation (plasma homocysteine and C-reactive protein [CRP]), as well as measures of vitamins folate and B12 that are necessary in the one-carbon cycle that includes homocysteine metabolism. Increased homocysteine and lower folate (markers of increased inflammation) are associated with cross-sectional cognitive deficits, whereas decreased folate alone may be a more sensitive measure for longitudinal differences (Kado et al., 2005). The several cardiovascular measures were additional covariates in the latent models to explain individual differences in regional change.

Specific Aim 3. Evaluate the indirect effects of age on cognitive decline mediated by regional anatomical changes.

3.1 Rationale. Iron accumulation is hypothesized as a cause for progressive cognitive declines in healthy aging mediated by decreased volumes. Cross-sectional differences in cognitive function have been associated with increased iron content in healthy aging and neurodegenerative disease. Longitudinal study of regional shrinkage supports differential neural anatomical changes that mediate age-related cognitive decline (Raz and Kennedy, 2009). Therefore, changes in regional iron content and subsequent atrophy may mediate the effects of age on cognitive decline. The present study modeled change in two different cognitive functions: working memory and spatial navigation. Verbal and non-verbal working memory measures are accepted markers of cognitive aging (Horn and Donaldson, 1980; Lindenberger et

al., 1993; Park, 2000) and are functional correlates of the hippocampus and striatum (Packard and Knowlton, 2002). Similarly, performance on spatial navigation tasks declines with age and deficits in spatial navigation correlate with regional differences in the hippocampus and striatum (Daugherty, master's thesis; see Moffat, 2009 for a review).

3.2 Methods. Due to limitations of sample size, this hypothesis was only tested in the larger lifespan sample with two measurement occasions. Participants completed verbal (listening span and *n*-back for digits) and non-verbal (spatial recall and *n*-back for objects) working memory tasks, and a spatial navigation task (virtual Morris water maze). These were added as additional outcome variables in the latent change score model analyses. As the lamina quadrigemina have no known direct contributions to working memory or spatial navigation functions, measures in these regions served as controls for model comparisons.

CHAPTER III
GENERAL METHODS

1. Participants

There were two lifespan samples both collected as part of larger longitudinal studies of cognitive and neural correlates of aging. The first sample (N = 89; 71% female) of healthy adults were age 19-77 years at baseline and were measured twice within two years (average delay = 25.07 months, *SD* = 2.11). The second sample (N = 32; 58% female) of healthy older adults were age 50-76 years at baseline and were assessed four times across 7 years (average delay between baseline and the first two follow-up assessments = 15.55 months, *SD* = 2.13; and between the 2nd and 3rd follow-up *M* = 60.33 months, *SD* = 8.82). See Tables 1 and 2 for demographic profiles of each sample.

Table 1. Demographic profile of Sample 1.

	Baseline	Follow-up
N	89	89
Age (years)	55.18 ± 12.85	57.23 ± 12.83
N of Hypertensive	17	19
Education (years)	15.70 ± 2.45	15.89 ± 2.93
MMSE	28.99 ± 1.02	28.92 ± 1.00
CESD	4.14 ± 4.21	4.47 ± 4.26

Table 2. Demographic profile of Sample 2.

	Baseline	1 st Follow-up	2 nd Follow-up	3 rd Follow-up
N	32	32	30	21
Age (years)	63.54 ± 9.35	64.85 ± 9.33	66.06 ± 9.15	71.27 ± 9.31
N of Hypertensive	7	9	10	9
Education (years)	16.28 ± 2.37	16.84 ± 2.67	16.90 ± 2.83	16.86 ± 2.69
MMSE	28.69 ± 1.23	28.44 ± 1.16	28.73 ± 1.02	28.52 ± 1.33
CESD	4.16 ± 4.22	3.84 ± 4.14	3.53 ± 3.19	3.29 ± 3.90

For both samples, participants were recruited from the greater Metro Detroit area and were consented following the University Human Investigations Committee guidelines. Participants were screened for neurological and cardiovascular pathology, thyroid disorder, psychiatric disease, drug and alcohol abuse, and head injury. Participants reported right-hand dominance (Edinburgh Handedness Questionnaire; Oldfield, 1971) and were screened for vision and hearing problems at each assessment. For inclusion at baseline, participants scored at least 26 on the mini-mental state examination (MMSE; Folstein et al., 1975) and less than 16 on a geriatric depression scale (CES-D; Radloff, 1977), and these measures were repeated at each assessment.

Sample 2 was selected for cases with at least two complete longitudinal data points of the four assessments. At the second follow-up, 2 participants were unwilling to participate, and at the last follow-up 10 participants declined participation, 1 participant had acquired a pacemaker and could not be scanned, and 1 participant had died of causes unrelated to cognitive status. The cases with missing data did not differ from those with complete data in baseline age ($t = -0.16$, $p = 0.87$) and education ($t = -1.55$, $p = 0.13$), or MMSE (all $t \leq 1.81$, $p \geq 0.09$), CESD (all $t \leq -1.50$, $p \geq 0.14$), and hypertension status (all $\chi^2 \leq 0.63$, $p \geq 0.43$) at any measurement occasion. Therefore, missing data were treated as missing at random and estimated with full information maximum likelihood in Mplus (Muthén et al., 1987), which is a well-established method to handle missing data in multi-level models (Larsen, 2011). Further, in the course of the longitudinal study, 9 participants developed conditions that would have been exclusionary at baseline: 2 participants developed bladder cancer, 1 participant a thyroid colloid cyst, 5 participants a heart condition (i.e., murmur, arrhythmia), and 1 participant reported possible binge drinking behaviors. In order to maintain the sample size, these 9 cases were kept for main

analyses and later excluded to determine if the main effects remained the same absent of these possible pathologies.

Finally, inclusion criteria of both samples allowed for current prescriptions of antihypertensive medications. In Sample 1, by the 2-year follow-up 8 participants were on a beta-blocker, another 11 on statins, and 6 on other anti-hypertensive medications. In Sample 2, by the last assessment 2 participants were on a beta-blocker, another 6 on statins, and 8 on other anti-hypertensive medications. Due to the low frequency of medication use in the total samples, these variables were not included as covariates in the models.

2. *T2* Relaxometry and Regional Volumetry*

The multi-echo susceptibility weighted image (SWI) sequence was acquired on a 4T Bruker Biospin scanner with Siemens interface for the first sample, and on a 1.5T Siemens Sonata scanner for the second sample. Due to the T2* dependence on the magnet field strength, data were measured and modeled for each sample separately.

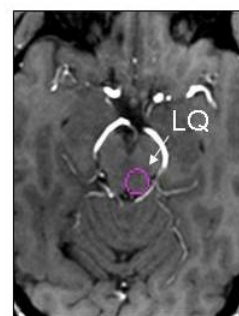
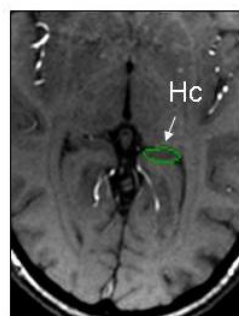
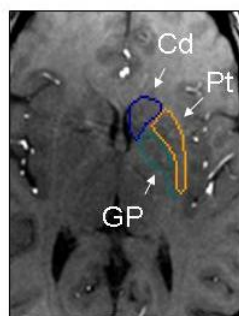
2.1 Image Acquisition. The SWI gradient-echo sequence for each sample was acquired with different parameters. For the first lifespan sample, the sequence consisted of 4 echoes (echo time, TE = 7.53-30 ms with an inter-echo interval of 7.5 ms). Other acquisition parameters were uniform across all echoes: 1 mm³ isotropic voxel; repetition time (TR) = 35 ms; flip angle (FA) = 25°; bandwidth = 200; field of view (FOV) = 256 x 208. During pre-processing, all images were interpolated to 1 × 1 × 1.5 mm voxel size, which improved the signal-to-noise ratio. In the second sample, 4 echoes were also collected (TE = 10-40 ms with an inter-echo interval of 10 ms), and other acquisition parameters were: 1 × 1 × 2 mm³ voxel; TR = 100 ms; FA = 30°; bandwidth = 170; FOV = 256 x 256. Noise was manually excluded from all measurements by applying a threshold that selectively isolated intensity values corresponding to image

inhomogeneity.

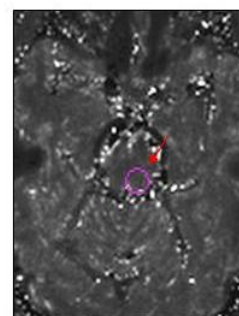
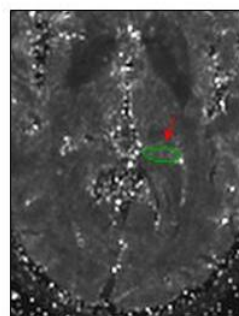
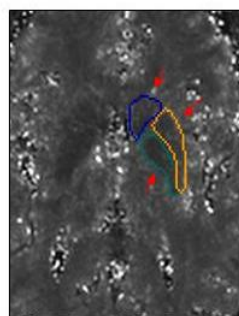
2.2 Pre-processing and Demarcation. All images were pre-processed in Signal Processing in NMR (SPIN) in-house written software: <http://www.mrc.wayne.edu/download.htm>. T2* maps were interpolated to common space and estimated by a maximum-likelihood fit function for exponential decay dependent upon TE. All boundaries were manually traced by a single rater (A.M.D) across all selected ROIs: hippocampus (Hc), caudate (Cd), globus pallidus (GP), putamen (Pt), and the lamina quadrigemina (LQ). Boundaries were marked on the first echo image as an anatomical reference and copied onto the T2* map. See Appendix A for a detailed description of the tracing procedures for each ROI and Figure 3 for examples of manual tracings. For each ROI, T2* was estimated as the average across all slices on which a given ROI was traced. Volumes were calculated as the sum of the traced region areas multiplied by the slice thickness, and adjusted for cranial size using the ANCOVA approach (Jack et al., 1989). Rater reliability was confirmed for all selected ROIs with an intra-class correlation coefficient (ICC(3); Shrout and Fleiss, 1979) exceeding 0.90 for volume and T2* in a sub-sample of 10 cases sampled twice with a delay of 2 weeks. T2* measures of iron were further validated by comparing baseline regional values measured from the 4T data with median post-mortem iron concentrations reported across studies (median values from Haacke et al., 2005; $R^2 = 0.86$) and age-based estimates after Hallgren and Sourander's (1958) lifespan post-mortem study ($R^2 = 0.99$; Figure 4).

4 T, 2 longitudinal measures

N = 89

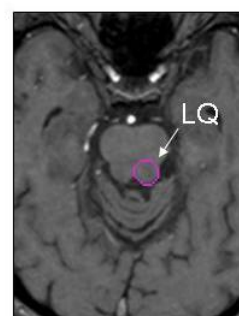
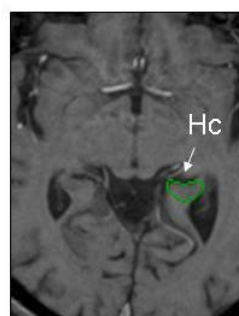
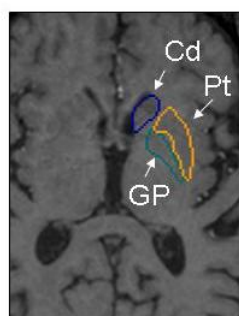
Anatomical
Reference
(TE = 7.53 ms)

T2* Map



1.5 T, 4 longitudinal measures

N = 32

Anatomical
Reference
(TE = 10 ms)

T2* Map

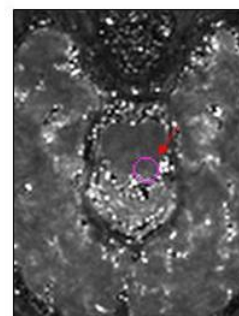
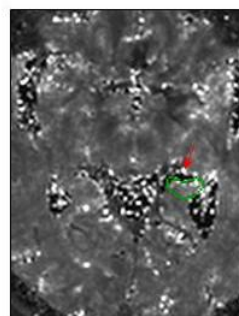
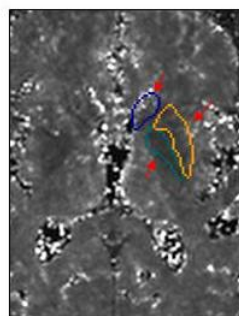
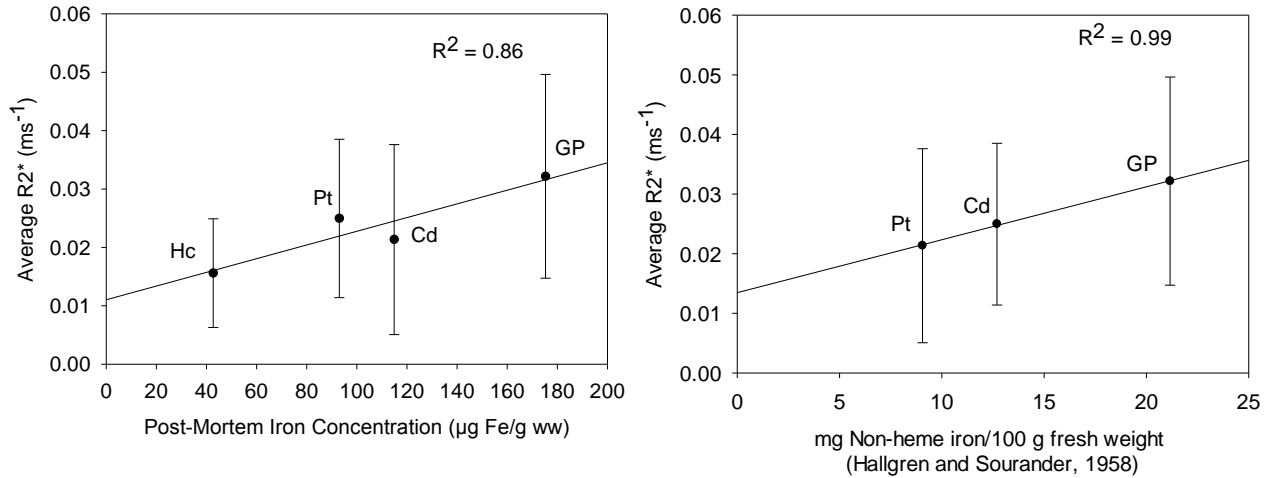


Figure 3. Example manual tracing on 4 T and 1.5 T images. Each ROI was manually traced on an anatomical reference image (first echo) and copied to T2* maps. On the T2*-weighted images, voxels representing high magnetic susceptibility (i.e., iron) are visualized with dark intensity. Cd—caudate nucleus, Pt—putamen, GP—globus pallidus, Hc—hippocampus, LQ—lamina quadrigemina.

Figure 4. Comparison of manually obtained T2* values (baseline 4T data) with median post-mortem measures reviewed in Haacke et al., 2005 and age-based estimates after Hallgren and Sourander, 1958. Error bars represent standard error of the mean.



3. Circulating Biomarkers of Cardiovascular Risk: Metabolic Syndrome and Pro-inflammatory Indicators

At MRI assessments, following a 12-hour overnight fast, several blood assays were collected from all subjects. The first lifespan sample had blood serum measures at both occasions, and the second sample had blood serum measures at the three longitudinal follow-up assessments. A metabolic syndrome factor (MetS) was computed as a composite of relevant indices (Grundy et al., 2005): blood serum high density lipoprotein cholesterol, total triglycerides, and glucose, as well as diagnosed or observed hypertension. Inflammation biomarkers measured in the blood samples were plasma total homocysteine (Hcy), and C-reactive protein, as well as folate and vitamin B12. Blood samples were collected close to the MRI site by venipuncture and 20 cc of whole blood were obtained in each draw. Samples were collected in serum separator tubes, except samples for Hcy that were collected in EDTA tubes, centrifuged to separate plasma and placed on ice. All analyses were performed at Detroit Medical Center laboratories. Hcy was determined by fluorescence polarization immunoassay,

and glucose and lipids enzymatically. All measures were treated as continuous in the present analyses.

4. Cognitive Assessment

Cognitive abilities were assessed in both samples, but due to the limitations of sample size, hypotheses pertaining to cognitive outcomes were only tested in the first lifespan sample. At baseline and follow-up, participants completed four working memory measures (two verbal and two non-verbal tasks) and a spatial navigation task as part of a larger battery of study.

4.1 Verbal Working Memory. The two verbal working memory measures were listening span and an N-back task. During listening span (LSPAN; Salthouse, Mitchell, Skovronek and Babcock, 1990), participants were required to answer simple questions about a sentence while simultaneously remembering the last word of the sentence. Sentences were presented in blocks of three trials, beginning with one test item per trial up to seven items per trial. An item was correct when the participant correctly answered the item question and recalled the word in the correct order as presented. Performance was scored as the sum total number correct across all trials (absolute span). This index was chosen because it presents more individual variability than simple span, but reduces chance error that is included in total span (Engle, Cantor, and Carullo, 1992). The estimated reliability of this measure is 0.90 (Salthouse, Skovronek and Babcock, 1990).

The second index was an N-back task (Dobbs and Rule, 1989; Hultsch, Hertzog, and Dixon, 1990) for digits. A randomly-ordered string of digits was presented to the participant, who was required to report the digit in the *n*th position. String lengths varied from 5 to 9 digits, and each digit was presented for 1500 ms. A screen prompting the participant's response immediately followed the last digit presented in the string. Participants were required to use a

number pad to respond. The task had three blocks of 20 trials each. In one block the participant reported the last digit seen (n position); the next block, the digit prior to the last ($n-1$); and the third block, the $n-2$ position. The order of block presentation was counter-balanced between individuals and across follow-up assessments. Performance was modeled as the proportion correct in the $n-2$ condition, as the other conditions are vulnerable to ceiling effects. The estimated reliability for this task is 0.91 (Salthouse, Hancock, Mainz, and Hambrick, 1996).

4.2 Non-Verbal Working Memory. Non-verbal working memory was measured with spatial recall and N-back tasks. The spatial recall measure was a computerized task modified from a task described by Salthouse (1994). Task stimuli were seven target squares within a 5×5 matrix that were marked with solid orange coloring. The configurations of target squares were randomly chosen, without repetition across trials. Each matrix was presented in the center of the screen for 3000 ms. Participants were instructed to memorize the locations of the target squares, and following the presentation, to mark the seven target squares each with an “X” in a 5×5 matrix provided as a printed test sheet. Performance was measured as the average number of correct recalled items across 25 trials. The estimated reliability of this task is 0.67 (Salthouse, 1994).

The second non-verbal working measure was an N-back task (Dobbs and Rule, 1989; Hultsch, Hertzog and Dixon, 1990) with stimuli selected from Kroll and Potter non-object norms (Kroll and Potter, 1984). Items were selected to minimally resemble real objects (mean rating = 5.89; 1—very much like a real object; 7—nothing like a real object). As in the verbal Nback task, there were three blocks of trials with 20 trials each. Items were presented for 2000 ms in strings varying in length from 5 to 9 items. Participants were asked to report the items in the n th, $n-1$, and $n-2$ positions. Participants reported items using a key pad to indicate the item as shown

on a prompt screen immediately following the last item of each string. Performance was measured as proportion correct in the $n-1$ position, as the n th position is vulnerable to ceiling effects and the $n-2$ to floor effects. The estimated reliability for this task is 0.88 (Salthouse, Hancock, Meinz, and Hambrick, 1996).

4.3 Spatial Navigation. Spatial navigation was measured in a computerized virtual Morris water maze (vMWM) task that was developed by Moffat and Resnick (2002). A detailed description of the virtual environment and testing procedures has been previously reported (Moffat et al., 2007). Briefly, the vMWM was presented as a circular pool within a larger room and the perimeter was surrounded by various objects (see Figure 5). Participants moved through the pool environment using a joystick and viewed the environment from a first-person perspective. The task was completed by repeatedly locating a platform that was “hidden”, but stationary across trials.

4.3.1 Testing procedures. Prior to placement in the vMWM pool, participants were trained to manipulate a joystick to travel within two unique virtual environments. To introduce the vMWM task, participants completed six practice trials in a vMWM that included a stationary platform that alternated between being hidden and visible on successive trials. Throughout the practice, participants were reminded that the environment remained the same and that the platform was stationary.

The testing vMWM included unique landmark cues, and the platform location was unique to the testing environment and was always “hidden”. The starting positions were in each of the three quadrants not containing the platform and were each repeated for a total of six trials. The search behavior was represented by changes in position recorded as a series of Cartesian coordinates in the virtual pool at a sampling rate of 100 Hz. No time limits were imposed on the

participants and each trial ended upon successfully locating the platform, which resulted in the platform lifting above the water plane with an audible signal.

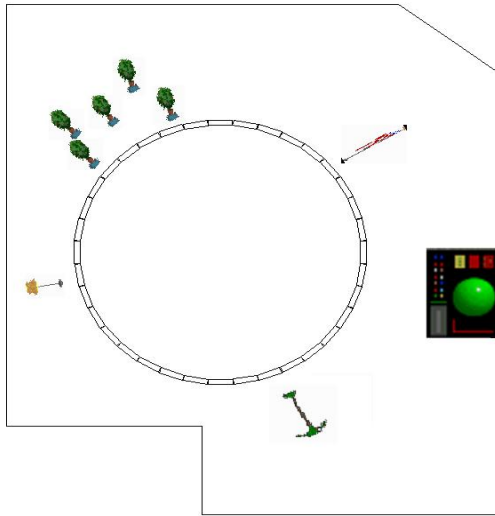


Figure 5. An over-head diagram of the test vMWM environment.

4.3.2 Navigation performance and control measures. Measures of spatial navigation included distance traveled from the start until the first platform intersection and the fractal dimensionality of the search path. Distance is a well-established measure of navigation efficiency (see Moffat, 2009 for a review) and fractal dimensionality of the search path is a proposed measure of path complexity from which we may infer qualities of an individual's cognitive map (Daugherty et al., 2014). Large distance traveled to the platform or high fractal dimensionality of the search paths are interpreted as deficits in spatial navigation. Fractal dimension was calculated from the Cartesian coordinates output using the FractalMean function in Fractal (v 5.20) software developed by Nams (Dalhousie University, <http://www.dal.ca/faculty/agriculture/environmental-sciences/faculty-staff/our-faculty/vilis-nams/fractal.html>). Fractal dimensionality was calculated by 1-slope of the function defined by change in $\log(\text{distance})$ and $\log(\text{spatial scale})$, and ranges from 1 (a straight line) to 2 (a line filling a two-dimensional plane; Nams, 2006). See Daugherty et al., 2014 for a detailed

description of the fractal dimension measure of path complexity. Navigation efficiency was modeled as the distance traveled on trials 1-3, 5, and 6 (omitting trial 4); and navigation complexity was measured as fractal dimensionality of trials 1-4 and 6 (omitting trial 5). Only 5 trials were used for each construct due to the inconsistency of the omitted trials with the overall learning curves in the whole sample.

Two control measures were used to assess possible age- and sex-related differences in proficiency with the joystick and prior experience with 3D virtual environments (e.g., video games). Following the place-navigation trials, the task was repeated in the same environment with a visible platform. Participants were instructed to move towards the visible platform as quickly as possible, and distance traveled was a measure of joystick control. In addition, based on a 7-point Likert rating (1—Never; 7—Every day), participants reported how often they played video games that displayed a 3D environment.

5. Longitudinal Structural Equation Modeling

Hypotheses were tested with longitudinal structural equation modeling: latent change score (LCSM; McArdle and Hamagami, 2001) and latent growth curve (LGCM; Preacher et al., 2008) models. Both modeling techniques incorporate an independent estimation of measurement error, a robust measurement of true longitudinal change and individual differences therein, and the incorporation of multiple variables. Latent models were estimated in Mplus (version 5.1, Muthén and Muthén, 2008). Prior to constructing latent variable models, univariate outliers in memory, blood assays, and anatomical measures were winsorized. All data were normed to baseline measures for the purpose of the analyses. To avoid spurious results related to limited sample size, simple effects models and indirect effects were bootstrapped with bias correction (5000 iterations of the whole sample; Hayes and Scharkow, 2013) to estimate 95% confidence

intervals (CI). Simple effects models estimated longitudinal change in a single factor without covariates. To test hypotheses of change in one factor preceding change in another, simple effects models were combined as parallel process models. Covariates were added to simple effect and parallel process models of regions that demonstrated significant variance in change. Nominal significance level was set at $p = 0.05$ and Bonferroni correction was used to adjust for multiple comparisons (Bonferroni α').

Nested models were constructed to estimate the hypothesized indirect and direct associations between regional T2*, volumetry, and cognitive functions with age, sex, cardiovascular risk and interactions therein as covariates. See Table 3 for a list of latent constructs and respective measures for identification. The indirect effect of change in iron on decline in cognition through regional shrinkage was tested according to the James and Brett (1984) method, in which a significant effect is sufficient to support an indirect relationship via the specified intermediate variable(s). Model fit was determined by accepted indices (Raykov and Marcoulides, 2006): normal theory weighted chi-square statistic (a non-significant value indicates good fit); the proportion of chi-square to degrees of freedom (less than 2 indicates good fit); root mean square error of approximation (RMSEA, a value equal to or less than 0.05 indicates excellent fit); comparative fit and Tucker-Lewis fit indices (CFI and TLI, respectively, values exceeding 0.90 indicate excellent fit); standardized root mean residual (SRMR, less than 0.05 supports good fit); and Akaike information criterion (AIC, comparatively smaller values indicate improved model fit). See Appendix C for examples of latent model construction.

5.2 Reverse Effects Models

To confirm the directionality of effects—i.e., the precedence of iron accumulation before volumetric shrinkage and subsequent cognitive decline—the structural regression pathways were

reversed. Due to the limitations of observational data without temporal precedence, causality between latent constructs cannot be confirmed. Yet, latent modeling techniques are confirmatory in nature, and regression structural pathways are unidirectional and imply causality. With the limitation to interpretation, the directionality of an association can be confirmed by testing a model that reverses the hypothesized relationship between variables. If the reverse effects models fit worse than the hypothesized models, then the directionality of the effects can be interpreted with greater confidence.

Table 3. Latent constructs and measures for identification in analyses.

Latent Construct	Measure (indicator)
<i>Regional Iron Content</i>	
1. Caudate Nucleus	Left & Right T2*
2. Putamen	Left & Right T2*
3. Globus Pallidus	Left & Right T2*
4. Hippocampus	Left & Right T2*
5. Lamina Quadrigemina	Left & Right T2*
<i>Regional Volumetry</i>	
1. Caudate Nucleus	Left & Right volume
2. Putamen	Left & Right volume
3. Globus Pallidus	Left & Right volume
4. Hippocampus	Left & Right volume
5. Lamina Quadrigemina	Left & Right volume
<i>Metabolic Syndrome</i>	
	Fasting blood glucose
	Total triglycerides
	High density lipoprotein cholesterol
	Hypertension status
<i>Inflammation</i>	
	Plasma homocysteine
	C-reactive protein
	Folate
	B12
<i>Cognition</i>	
1. Verbal Working Memory	Listening span
	N-back for digits
2. Non-Verbal Working Memory	Spatial recall
	N-back for objects
3. Spatial Navigation Efficiency	5 trials, Distance
4. Spatial Navigation Complexity	5 trials, Fractal dimension of search path

CHAPTER IV

RESULTS

1. Accumulation of Iron and Decline in Volume (Aim 1)

1.1 Sample 1 (two occasions). Change in regional iron and volume were initially tested in simple effects latent change score models, without covariates. All simple effects models had excellent fit according to multiple goodness-of-fit indices: $\chi^2 \leq 11.15$, $p \geq 0.13$; RMSEA ≤ 0.08 ; CFI ≥ 0.98 ; SRMR < 0.08 . Iron content significantly increased in all regions (see Table 3), except for the Hc (mean change = 0.14, $p = 0.19$) and the effect in the LQ did not pass criteria for multiple comparison correction (mean change = -0.26, $p = 0.03$; $\alpha' = 0.01$). The magnitude of change did not differ among regions that evidenced change in iron content (all $p \geq 0.34$). Despite the observed mean change, the rank order of regions by their average iron content remained the same: the GP had the most iron, followed by the Pt and Cd, and notably less iron in the Hc and LQ (all $p < 0.001$; see Figure 6).

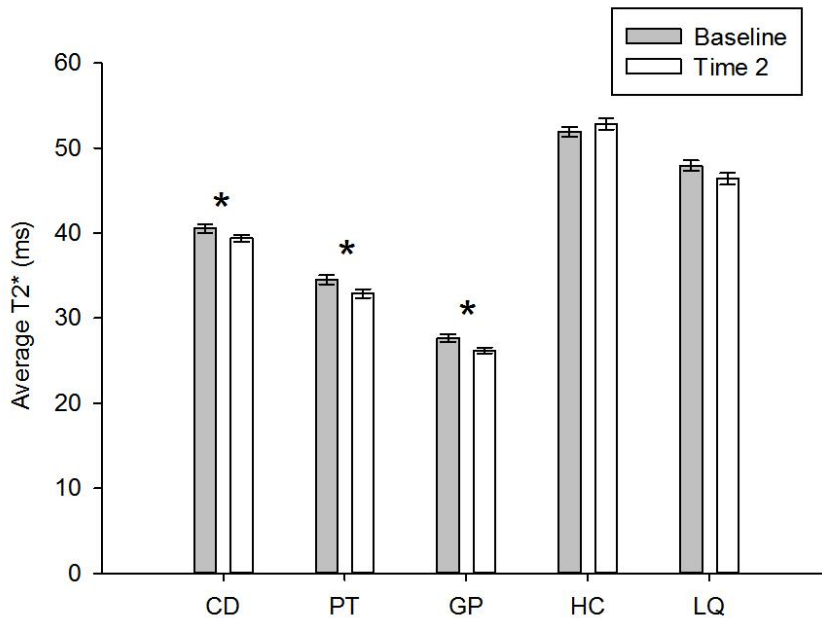


Figure 6. Sample 1 regional average T2* at baseline and at 2-year follow-up. Error bars represent standard error of the mean; * $p < 0.01$.

All regions, except the GP and LQ, significantly declined in volume, whereas LQ evidenced volume increase (see Table 4). Significant individual differences in the regional iron content and volume of the striatum and Hc (variance in change ≥ 0.39 , all $p < 0.01$) justified further analyses seeking factors that account for the observed variability. Therefore, additional latent change score models tested whether the increase in iron content preceded decline in regional volume. The models included baseline age, MetS and inflammation biomarkers as covariates.

Table 4. Sample 1: Two-year mean change and variance in change in regional iron and volume.

ROI	Measure	Mean	95% CI	d	Variance in	Variance in
		Change	Mean Change		Change	Intercept
Caudate	T2*	-0.26 *	-0.38/-0.16	-0.29	0.39 *	0.80 *
	Volume	-0.51 *	-0.64/-0.40	-0.55	0.62 *	0.85 *
Globus Pallidus	T2*	-0.33 *	-0.43/-0.22	-0.38	0.60 *	0.76 *
	Volume	0.11	0.002/0.23	0.13	0.27 †	0.75 *
Putamen	T2*	-0.33 *	-0.45/-0.20	-0.36	0.53 *	0.82 *
	Volume	-0.64 *	-0.76/-0.51	-0.74	0.67 *	0.75 *
Hippocampus	T2*	0.14	-0.05/0.32	0.17	0.99 *	0.66 *
	Volume	-0.70 *	-0.81/-0.60	-0.90	0.36 *	0.61 *
Lamina						
Quadrigemina	T2*	-0.26 †	-0.44/-0.07	-0.28	0.99 *	0.86 *
	Volume	0.53 *	0.38/0.67	0.64	0.32 †	0.68 *

Note: Unstandardized coefficients are reported for data normed to baseline. 95% confidence intervals are bootstrapped with bias-correction. d is an effect size estimation of mean change calculated = Mean Change / $\sqrt{\text{Variance in Intercept}}$. * $p < 0.01$; † nominal $p < 0.05$ that does not maintain significance after correction for multiples comparisons.

1.2 Sample 2 (four occasions). A similar pattern of effects was observed in the second lifespan sample with four longitudinal measurements across 7 years. All simple effects models had good fit according to multiple goodness-of-fit indices: $\chi^2 \leq 44.13$, $p \geq 0.08$; RMSEA ≤ 0.12 ;

CFI \geq 0.90; SRMR $<$ 0.14. Iron significantly increased in the GP (mean change = -0.15, $p <$ 0.001). However, the effect in the Pt failed to maintain significance after Bonferroni correction (mean change = -0.12, $p = 0.04$; $\alpha' = 0.01$), and there was no significant change in the Cd (see Table 5). Although iron did not significantly change in these regions, volumes did shrink (all $p <$ 0.01) to suggest an increase in relative concentration. As observed in the first sample, Hc volume decreased (mean change = -0.65, $p <$ 0.001), but iron content remained unchanged (mean change = -0.14, $p = 0.49$).

Table 5. Sample 2: Seven-year mean change and variance in change in regional iron content and volume.

ROI	Measure	Mean Change	95% CI Mean Change	d	Variance in Change	Variance in Intercept
Caudate	T2*	0.07	-0.03/0.07	0.11	0.03	0.40 †
	Volume	-0.69 *	-0.90/-0.49	-0.70	0.06 †	0.98 *
Putamen	T2*	-0.12 †	-0.21/-0.03	-0.12	0.07 *	1.00 *
	Volume	-0.40 *	-0.50/-0.29	-0.38	0.06 *	1.13 *
Globus Pallidus	T2*	-0.15 *	-0.26/-0.03	-0.20	0.04	0.54
	Volume	-0.37 *	-0.51/-0.24	-0.59	0.07	0.40
Hippocampus	T2*	-0.14	-0.38/0.11	-0.12	0.49 *	1.42 *
	Volume	-0.65 *	-0.71/-0.59	-1.30	0.02 †	0.25 *
Lamina						
Quadrigemina	T2*	0.15	-0.01/0.31	0.12	0.14 *	1.48 *
	Volume	-0.44 *	-0.59/-0.30	-0.51	0.04	0.75

Note: Unstandardized coefficients are reported for data normed to baseline. 95% confidence intervals are bootstrapped with bias-correction. d is an effect size estimation of mean change calculated = Mean Change / $\sqrt{\text{Variance in Intercept}}$. * $p <$ 0.01; † nominal $p <$ 0.05 that does not maintain significance after correction for multiples comparisons.

2. Accumulation of Iron Was Associated with Decline in Volume (Aim 1)

2.1 *Sample 1 (two occasions)*. Models including change in striatal and Hc iron content, volume, and cardiovascular risk covariates fit well: all $\chi^2 \leq 359.09$, $p \geq 0.22$; RMSEA ≤ 0.03 ; CFI ≥ 0.89 ; WRMR < 0.83 . Accumulation of iron was associated with volumetric decline only in the striatum: Cd ($\beta = 0.49$, $p = 0.002$; $\alpha' = 0.02$) and Pt ($\beta = 0.31$, $p = 0.003$; Bonferroni $\alpha' = 0.01$). Smaller baseline volumes were associated with slower shrinkage in Cd ($\beta = -0.91$, $p < 0.001$; $\alpha' = 0.02$) and Pt ($\beta = -0.87$, $p < 0.001$; $\alpha' = 0.02$). A similar effect was noted in iron content estimates: greater iron content at baseline was associated with slower accumulation in the Cd ($\beta = -0.45$, $p < 0.05$) and the effect in the Pt ($\beta = -0.13$, $p = 0.05$) showed a non-significant trend in the same direction.

Advanced age was associated with more Cd iron ($r = -0.56$, $p < 0.001$; $\alpha' = 0.02$) and smaller volume ($r = -0.28$, $p = 0.02$; $\alpha' = 0.02$) at baseline. Similarly, at baseline older adults had more Pt iron ($r = -0.33$, $p = 0.003$; $\alpha' = 0.02$) and smaller Pt volumes ($r = -0.26$, $p = 0.03$), although the later effect did not maintain significance after Bonferroni correction ($\alpha' = 0.02$). The association between baseline age and striatum iron content was larger than that between age and striatum volumes (Steiger $Z = 7.17$ and 3.95 , $p < 0.001$, for Cd and Pt, respectively). Taken together, the accumulation of iron in the striatum accounted for age-related volumetric decline and the change in both factors was attenuated in later life. Further, there was an indirect association between baseline iron content and change in volume in the Pt (standardized indirect effect = -0.27 , $p = 0.01$; $\alpha' = 0.02$; 95% CI: $-0.49/-0.04$) and a trend in the Cd (standardized indirect effect = -0.22 , $p = 0.07$; 95% CI: $-0.39/-0.12$), although the bootstrapped 95% confidence intervals suggest that the test of the latter effect was under-powered. Thus, high

baseline iron content in these regions predicted later volumetric decline. See Figure 7 for individual change trajectories in striatal volumes and T2*.

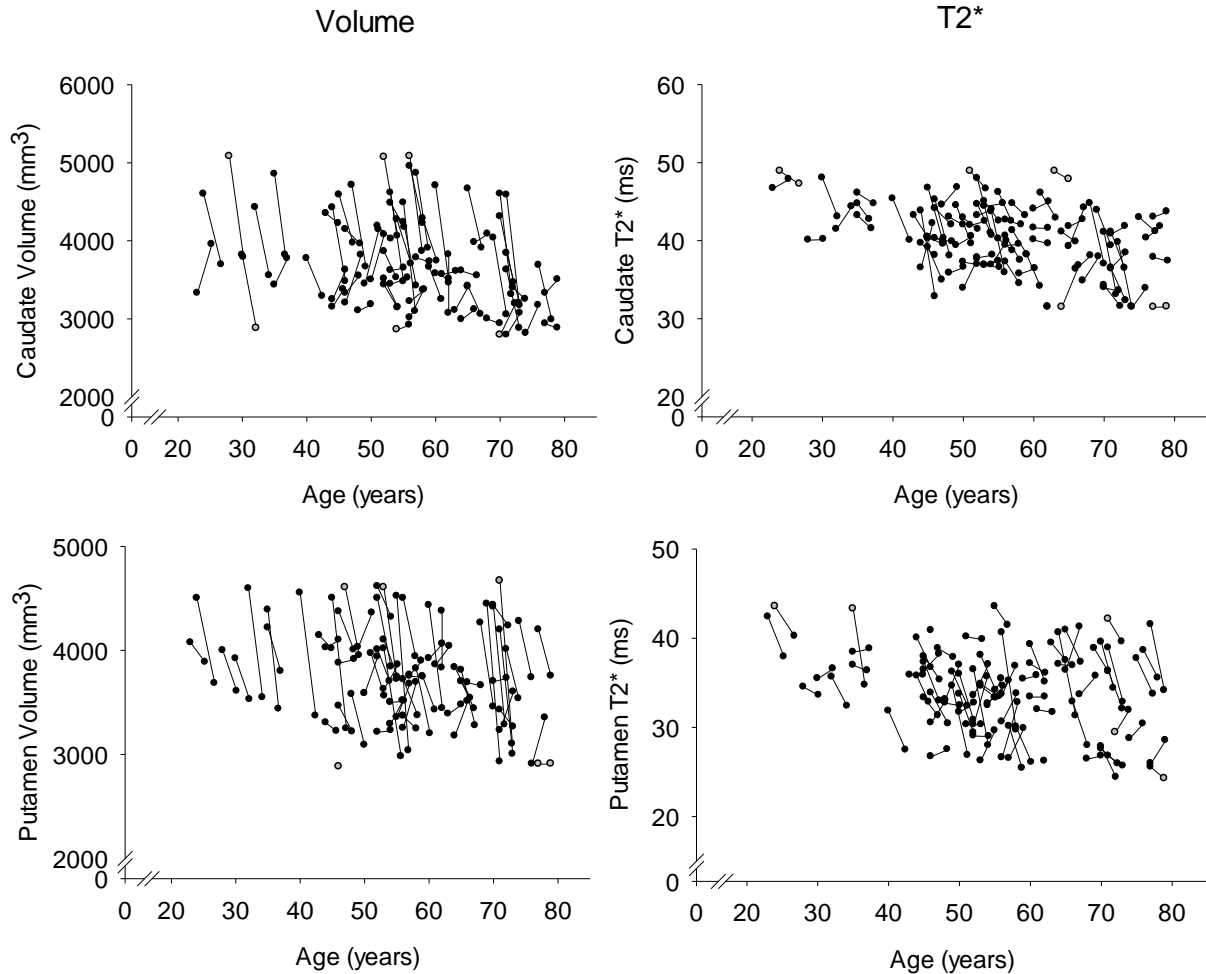


Figure 7. Sample 1 individual trajectories of two-year change in striatal volume and iron across the lifespan. Gray circles represent data points that were winsorized.

In contrast to the striatum, baseline iron content in the Hc was unrelated to shrinkage. Hc iron did not change and individual differences in Hc iron content were associated neither with volume at baseline ($r = -0.02$, $p = 0.83$) nor with Hc shrinkage over time ($\beta = 0.11$, $p = 0.41$). Advanced age was associated with greater iron content in the Hc at baseline ($r = -0.26$, $p = 0.02$;

$\alpha' = 0.02$), but not with the baseline volume ($r = -0.09$, $p = 0.34$). Similar to the striatum, the initial (baseline) values limited subsequent decline in the Hc. Larger Hc iron content ($r = -0.41$, $p = 0.02$; $\alpha' = 0.02$) and smaller volume ($r = -0.37$, $p = 0.01$; $\alpha' = 0.02$) limited the degree of change in each of these factors. Therefore, individual differences at baseline partially accounted for variability in change over time.

For the sole purpose of a control comparison, the LQ model was estimated and had poorer fit than models of the other regions: $\chi^2 = 0.83$, $p = 0.17$; RMSEA = 0.03; CFI = 0.83; WRMR = 0.87. LQ iron was unrelated to volume at baseline ($r = 0.01$, $p = 0.84$) and did not account for change in volume across time ($\beta = -0.17$, $p = 0.15$). Further, age was not associated with either factor at baseline ($r = -0.16$ and -0.14 , $p \geq 0.15$, iron and volume, respectively). Finally, sex did not account for individual differences in striatal or Hc regional measures (all $p \geq 0.06$; $\alpha' = 0.02$).

2.2 Sample 2 (four occasions). The association between baseline values and subsequent change was replicated in the second sample. Larger volume at baseline in the Pt ($r = -0.25$, $p = 0.01$; $\alpha' = 0.01$), Hc ($r = -0.06$, $p = 0.002$; $\alpha' = 0.01$), and a trend in the Cd ($r = -0.21$, $p = 0.05$) was associated with greater longitudinal declines; but the same effect was not observed in the GP ($r = -0.14$, $p = 0.17$) or LQ ($r = -0.15$, $p = 0.38$). The limiting effect of baseline on iron accumulation in the Pt was marginally significant ($r = -0.11$, $p = 0.05$), but not in the GP ($r = -0.07$, $p = 0.44$). See figures 8 and 9 for individual change trajectories in GP and Pt iron and volumes. Removal of the 9 participants who had developed exclusionary conditions in the course of the study did not change the original significant effects (all $p < 0.01$). The precedence of iron accumulation on volumetric shrinkage was not tested in the second sample, as no region

demonstrated simultaneous change in iron and volume, with significant variance in volumetric change.

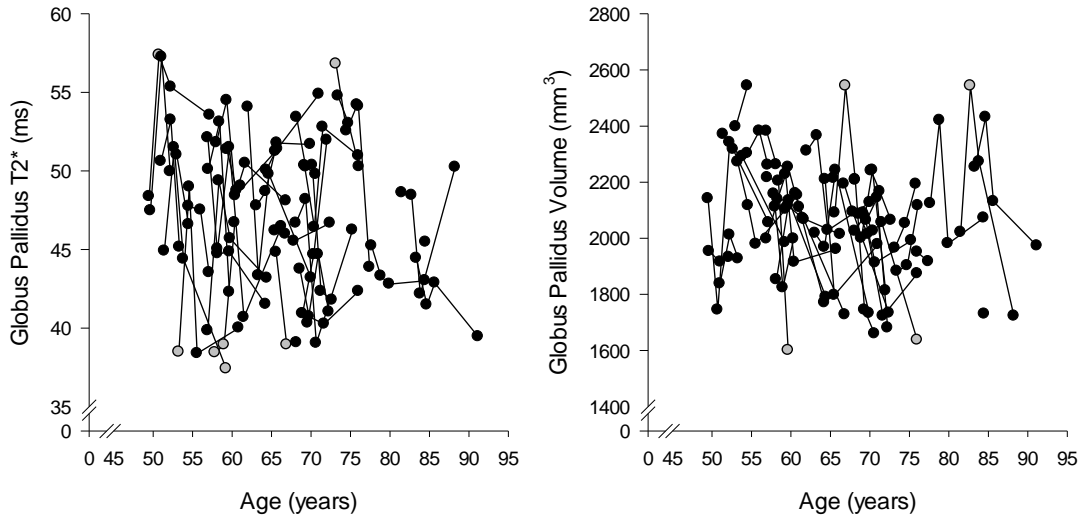


Figure 8. Sample 2: individual trajectories of seven-year change in globus pallidus volume and iron across the lifespan. Gray circles represent data points that were winsorized.

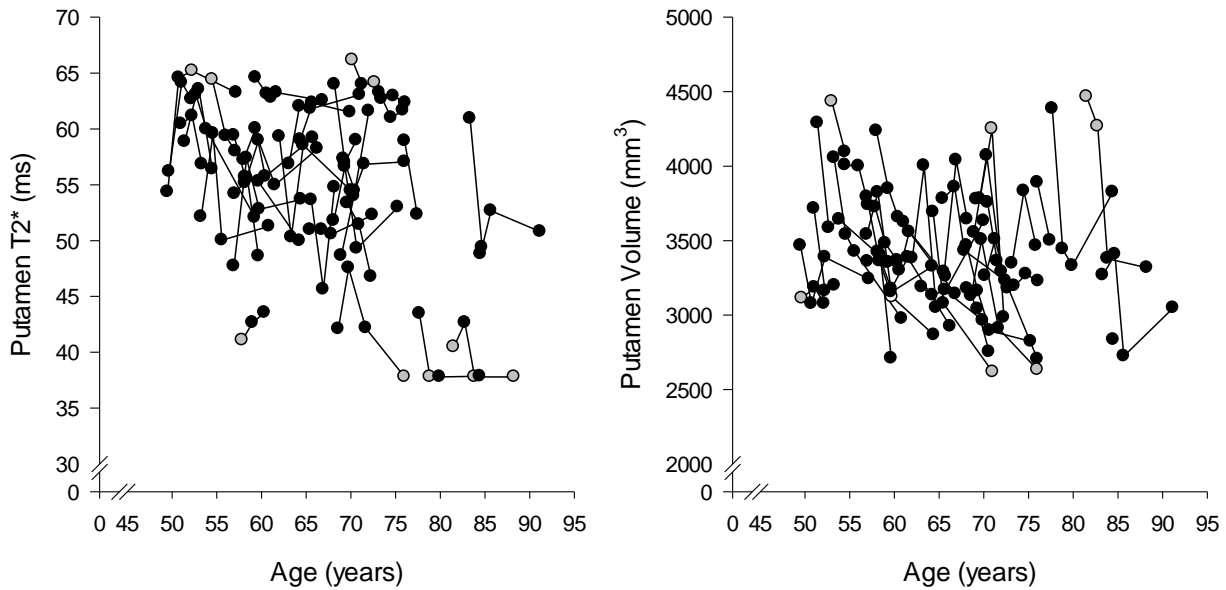


Figure 9. Sample 2: individual trajectories of seven-year change in putamen volume and iron across the lifespan. Gray circles represent data points that were winsorized.

3. Increased Cardiovascular Risk was Associated with Greater Iron Content at Baseline (Aim 2)

Cardiovascular risk was modeled as two latent factors: MetS and inflammation. Neither factor significantly changed longitudinally in either sample (all $p > 0.10$). Therefore, each factor was modeled as time invariant.

3.1 Sample 1 (two occasions). Higher MetS factor score was associated with greater baseline iron content in the Cd ($\beta = -0.33$, $p = 0.003$; $\alpha' = 0.02$), and the effect in the Pt did not meet criteria for multiple comparison correction ($\beta = -0.25$, $p = 0.04$; $\alpha' = 0.02$). Independent of the regional iron content, higher MetS score was associated with smaller baseline Pt volume ($r = -0.23$, $p = 0.01$; $\alpha' = 0.02$) but not Cd volume ($r = -0.09$, $p = 0.31$). As was previously described, differences at baseline were associated with variability in change. An increase in MetS score correlated with greater iron content and smaller volume in the striatum at baseline, which independently accounted for attenuated decline over time. However, the indirect associations between baseline MetS score and change in regional iron content and volume were not significant (all $p \geq 0.10$). Therefore, MetS risk explained individual differences in the striatum at baseline, but did not independently account for individual differences in change.

Metabolic syndrome score was unrelated to measures of the Hc (all $p \geq 0.55$). Elevation in MetS score correlated with higher baseline iron in the LQ ($r = -0.33$, $p = 0.02$), but not with other measures in that region (all $p \geq 0.38$). Inflammation score was unrelated to iron content or volumes in any region (all $p \geq 0.24$). Advanced age was associated with higher MetS score (4.63, $p = 0.002$) and men had a higher score (-0.29, $p = 0.01$). But age (-0.81, $p = 0.35$) and sex (-0.07, $p = 0.24$) were unrelated to inflammation scores.

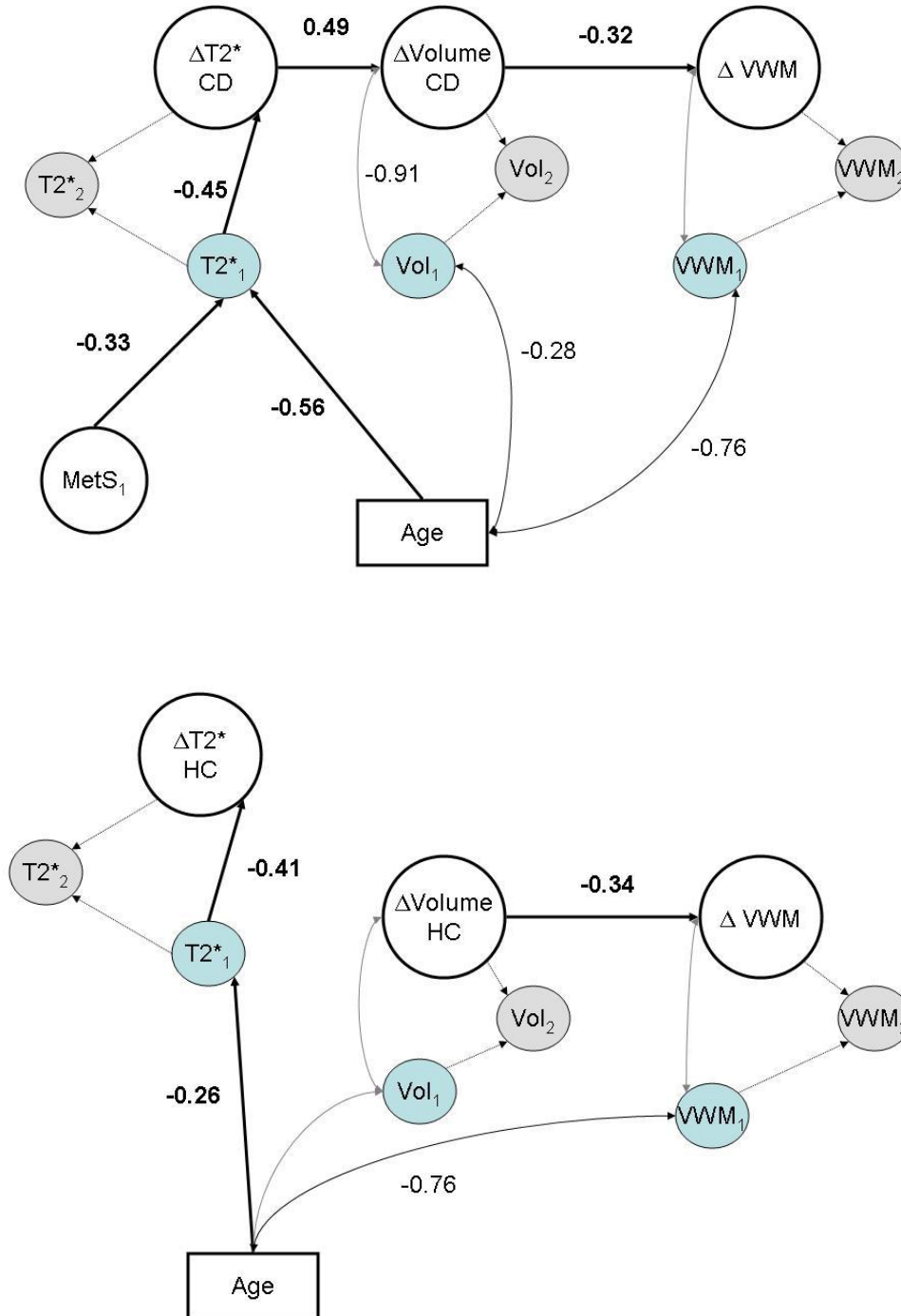
3.2 *Sample 2 (four occasions)*. In the second sample, neither metabolic syndrome nor inflammation accounted for individual differences in Pt or Hc iron (all $\beta \leq 2.41$, all $p \geq 0.58$) or volume (all $\beta \leq -0.42$, all $p \geq 0.71$).

4. Less Improvement in Working Memory was Associated with Regional Iron and Volume (Aim 3)

Working memory was assessed in verbal and non-verbal domains in Sample 1. Simple effects models for change in working memory fit very well: all $\chi^2 \leq 6.53$, $p \geq 0.37$; RMSEA ≤ 0.03 ; CFI = 1.00; SRMR ≤ 0.07 . Non-verbal working memory did not change (mean change = -0.02, $p = 0.76$; 95% CI: -0.10/0.07), nor was there significant variability in change ($\sigma = 0.01$, $p = 0.85$). Therefore, this construct was not considered in the remainder of the analyses.

Verbal working memory significantly improved after the two-year delay (mean change = 0.23, $p < 0.001$; 95% CI: 0.14/0.34), and individuals varied in verbal working memory at baseline ($\sigma = 0.46$, $p = 0.004$), but not in the magnitude of change ($\sigma = 0.05$, $p = 0.49$). Poorer verbal working memory at baseline was associated with advanced age ($\beta = -0.76$, $p < 0.001$), and, marginally, with smaller Cd volume ($\beta = 0.18$, $p = 0.05$). Declines in Cd and Hc volumes were associated with lesser improvement in verbal working memory: $\beta = -0.32$, $p = 0.02$; $\beta = -0.34$, $p = 0.01$, respectively (Figure 10). Cd ($\beta = 0.21$, $p = 0.17$) and Hc ($\beta = 0.11$, $p = 0.56$) iron content was unrelated to baseline performance. The indirect effect of baseline Cd iron on change in verbal working memory failed to reach significance (standardized indirect effect = -0.35, $p = 0.06$). Thus, accumulation of iron accounted for regional volumetric shrinkage, but did not independently explain change in verbal working memory.

Figure 10. Simplified parallel process latent change score models of Cd and Hc iron and volume effects on verbal working memory. Δ indicates latent change; MetS—metabolic syndrome factor, Vol—volume, VWM—verbal working memory.



5. Decline in Spatial Navigation Efficiency was Associated with Increased Iron, not Shrinkage (Aim 3)

Learning slopes in vMWM navigation were measured as navigation complexity and navigation efficiency in Sample 1. The models examined change in learning slopes across 5 repeated trials comparing baseline to the 2-year follow-up, while controlling for potential individual differences in the first trial. The simple effects models for spatial navigation complexity and efficiency had excellent fit: all $\chi^2 \leq 39.66$, $p \geq 0.27$; RMSEA < 0.04 ; CFI ≥ 0.95 ; SRMR < 0.09 . The learning slopes of navigation complexity, or fractal dimensionality of the search paths, did not change (mean change = 0.12, $p = 0.38$; 95% CI: -0.10/0.36), nor were there significant individual differences in change ($\sigma = 0.16$, $p = 0.14$). Learning slopes in navigation efficiency, or distance traveled from the start to the platform, did change (mean change = 0.21, $p = 0.04$; 95% CI: 0.07/0.48). Examination of the 95% confidence intervals suggests individual differences in baseline learning ($\sigma = 0.03$, $p = 0.24$; 95% CI: 0.002/0.13), and marginal individual differences in change over time ($\sigma = 0.03$, $p = 0.31$; 95% CI: 0.00/0.17). Therefore, additional models were estimated to test the contribution of regional iron content and volumes to baseline spatial navigation efficiency and subsequent change.

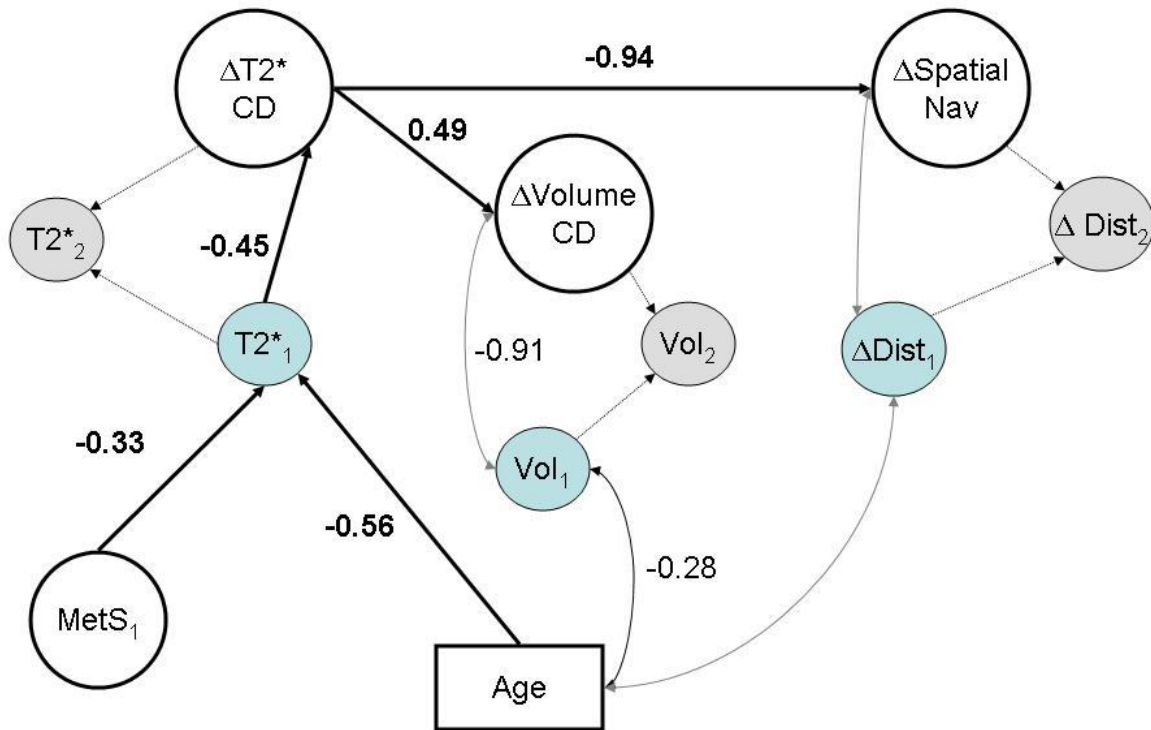
Parallel process latent change score models that included the effects of regional iron accumulation and volumetric shrinkage on spatial navigation efficiency, with cardiovascular risk factors and age covariates fit well: all $\chi^2 \leq 530.81$, $p \geq 0.31$; RMSEA < 0.02 ; CFI ≥ 0.90 ; SRMR < 0.89 . Baseline slope was unrelated to baseline Cd iron content ($r = -0.04$, $p = 0.11$) or volume ($r = -0.03$, $p = 0.12$), and these were constrained in the final model. There was a non-significant trend for an association between the accumulation of iron in the Cd and lesser improvement at follow-up ($\beta = -0.94$, $p < 0.06$; 95% CI: -1.91/-0.28), and examination of the bootstrapped 95%

confidence intervals suggests that the test of this effect was under-powered in the present sample (see Figure 11). Change in Cd volume was not related to change in vMWM performance ($\beta = 0.09$, $p = 0.28$). Differences in longitudinal change in Hc iron ($\beta = -0.02$, $p = 0.53$) and volume ($\beta = 0.01$, $p = 0.88$) were unrelated to longitudinal change in spatial navigation efficiency. Iron content and volumes of other ROIs were also not significant predictors (all $p \geq 0.25$). Advanced age was associated with less efficient performance on the first trial ($\beta = 0.01$, $p < 0.001$), but not with baseline learning slope ($r = 0.54$, $p = 0.17$). MetS score, inflammation, and sex were not independently related to spatial navigation performance (all $p \geq 0.13$), and these paths were constrained in the final models. There were no significant age- or sex-related differences in the vMWM control measures: joystick control (all $p \geq 0.22$) or experience with 3D video games (all $p > 0.68$); and in the interest of parsimony, these variables were excluded from the latent models.

6. Reverse Effects Models

To test the directionality of effects—i.e., the precedence of iron accumulation before volumetric shrinkage and subsequent cognitive decline—the structural regression pathways were reversed. All reverse effects models fit worse than the hypothesized models: all $\chi^2 \geq 572.95$, $p \leq 0.16$; RMSEA > 0.03 ; CFI ≤ 0.82 ; SRMR > 0.91 .

Figure 11. Simplified parallel process latent change score model of Cd iron and volume effects on spatial navigation efficiency (distance to platform). Δ indicates latent change; Met—metabolic syndrome factor, Vol—volume, Dist—distance.



CHAPTER V

DISCUSSION

More than a half-century ago, the accumulation of free non-heme iron in the brain was proposed as a mechanism to explain neural and cognitive decline in aging and disease (Harman, 1956). The present study provides the first longitudinal evidence for iron accumulation in normal aging. Further, regional accumulation of iron over a two-year span partially explained volumetric shrinkage and cognitive changes—accepted hallmarks of aging.

As has been observed before, regions differed in iron content. The basal ganglia have large concentrations of iron persistently across the lifespan. Based on post-mortem measures, iron appears to increase exponentially in the basal ganglia during child development (Hallgren and Sourander, 1958), and as shown here, regional iron continues to accumulate into later life. Based on cross-sectional studies, iron was thought to preferentially increase in the striatum (see Daugherty and Raz, 2013 for a review), but this was not observed in the patterns of longitudinal change. Despite longitudinal increase, the rank order of regional iron content was maintained: the GP had the largest content, followed by the striatum, and notably less in the Hc and LQ.

Regional differences in iron content may be due to metabolic demands of neural function. For example, dopamine transmission is dependent upon non-heme iron (Berg et al., 2007), and regions that are rich in iron express dopamine: the basal ganglia (Rice, Patel, and Crag, 2013; Packard and Knowlton, 2002; Martin, Ye, and Allen, 1998), the red nucleus and the substantia nigra (see Daugherty and Raz, 2013 and Zecca et al., 2004 for reviews; Packard and Knowlton, 2002). Diseases diagnosed by abnormally high iron content in these regions often present with motor dysfunction that is also dopamine-dependent (Rice, Patel, and Crag, 2013; see Zecca et al., 2004 for a review). Taken together, these observations suggest that non-heme iron in the brain

supports dopaminergic function. Therefore, accumulation of iron in the basal ganglia may occur initially to meet the metabolic demands of neural transmission (see Mills et al., 2010). Eventually iron metabolism becomes either corrupted or insufficient to manage the large concentrations (Hare et al., 2013), leading to an unchecked increase in free iron. An unregulated accumulation of non-heme iron will promote oxidative stress that can disrupt neural function (see Zecca et al., 2004; Mills et al., 2010 for reviews). Because the trajectory of change appears to be monotonic, it is unclear at which point in the lifespan iron accumulation stops being adaptive and instead becomes a harbinger of impairment.

In addition to disrupting neural transmission, increased iron content may cause neural atrophy via oxidative stress. Non-heme iron accumulation outside of ferritin sequestration accelerates apoptosis and is a proposed mechanism to explain regional shrinkage (see Bartzokis, 2011; Mills et al., 2010 for reviews). As evidenced here, shrinkage of the striatum followed accumulation of iron in these regions. The association between longitudinal changes in iron content and volume was observed only in the striatum; differences in iron content were unrelated to Hc and GP volumes. However, at baseline, high iron content in the Hc and GP was associated with smaller volumes, similar to what has been reported in extant cross-sectional studies (Rodrigue et al., 2012; 2011; Cherubini et al., 2009). It is plausible that iron-related shrinkage may be observed in these regions with a longer delay than two years. Yet, in the second sample with measurements over 7 years, there were no individual differences in GP volume shrinkage, nor a significant change in Hc iron, and thus this hypothesis could not be further tested. The second sample was limited to adults 50 years and older, which omitted age-related variability in earlier adulthood; lacking this contrast, the magnitude of individual differences in later life may be reduced. Thus, a larger lifespan sample with long delays may identify iron-related shrinkage

in extra-striatal regions. Nonetheless, regional iron accumulation was observed in both samples, and there were significant individual differences in change.

Individual differences in iron-related shrinkage were in part explained by increase in cardiovascular risk factors. Elevation in MetS score was associated with increased iron content in the striatum at baseline. Metabolic syndrome compromises blood flow to the brain, interrupting the delivery of necessary oxygen and metabolites (Grundy et al., 2005). A decrease in iron metabolites that are delivered via vascular supply may lead to regional accumulation of iron (Hare et al., 2013). In addition, the brain vascular endothelium regulates brain iron transport (Deane et al., 2004) and a decrease in blood flow may lead to iron mired within regions, increasing the risk to oxidative stress. Thus, poor cardiovascular health—even subclinical elevations in risk factors—increases the likelihood of iron-related atrophy.

Increased cardiovascular risk has been reported to exacerbate age-related brain shrinkage (Rodrigue et al., 2011; Raz et al., 2005; Raz, 2004), but the mechanism by which this effect occurs is unclear. Possibly, increased cardiovascular risk causes an increase in iron-related oxidative stress to affect volume. Elevations in MetS score were associated with higher baseline iron content, which in turn accounted for individual differences in the changes in iron and volume. However, the MetS factor did not selectively act through iron content—higher MetS score was independently associated with decline in Pt volume. Thus, MetS risk may be a non-specific factor that increases vulnerability to iron-related atrophy amongst other age correlates.

Higher MetS was associated with greater risk for decline, but the rate of change in iron and volume was limited by the baseline state. Observed in both longitudinal samples, persons with greater iron at baseline did not accumulate as much over time compared to those with lower levels. Similarly, smaller volumes at baseline were associated with less shrinkage over time.

Greater iron and smaller volumes at baseline were associated with advanced age and MetS, and this constellation of factors limited subsequent change in regional measures. In other words, elevations in the MetS factor may increase the risk for iron-related atrophy, but decline in healthy adults is constrained by a threshold that likely distinguishes aging from disease. Indeed, the smaller effect sizes in the second older sample may support a non-linearity in lifespan change. Whereas attenuated iron accumulation may be due to saturation, attenuated shrinkage suggests neural resiliency. If interpreted as independent mechanisms, these two effects appear to be in opposing directions. Yet, when considered together as part of a singular mechanism of decline, staved change in either factor limits the degree of global decline.

This is incongruent with an alternative hypothesis of brain reserve in aging (Satz, 1993), which posits that larger brain volumes would be associated with lesser decline, not greater. The evidence for the brain reserve hypothesis has been inconsistent in studies of healthy aging (Raz et al., 2005; 2010), but there is greater support from studies of clinical dementia and Alzheimer's disease (see Valenzuela, 2008; Fratiglioni and Wang, 2007 for reviews). Thus, the inconsistencies may be attributable to a distinction between normal aging and disease. Because symptoms of age-related neurodegenerative disease present along a continuum that overlaps with normal age-related declines (Walters, 2011; Petersen et al., 2011; Petersen et al., 1999), it is an immediate research interest to distinguish healthy aging from prodromal disease. This intriguing challenge is best aided by studies of aging selecting samples with optimal health, even excluding relatively common age-concomitant pathologies. In such samples (e.g., Raz et al., 2010) there is evidence for a threshold between healthy aging and disease, and absent of pathology, healthy adults may not pass this threshold.

In the present study, an attenuation of the rate of change in both iron and volume further supports the hypothesis of a threshold between healthy aging and disease. Normal aging appears to be characterized by moderate increase in iron and declines in volume. The degree of decline may be larger in diseases such as Alzheimer's disease (Bartzokis, 2011) or multiple sclerosis (Walsh et al., 2014). In these diseases and aging, iron accumulation has been proposed as a mechanism of global brain decline and related cognitive deficits (see Bartzokis, 2011; Zecca et al., 2004 for reviews).

Here, iron accumulation was related to individual differences in longitudinal change in cognition, namely in verbal working memory and spatial navigation. Verbal working memory improved over time, independent of age. This is typical of memory tasks that can benefit from repeated exposure, or retest effects (Thorvaldsson et al., 2005). However, greater accumulation of iron in the Cd limited the degree of improvement in memory. This effect was associated with advanced age—older adults who had more iron at baseline benefited less from retest compared to their younger counterparts with less iron. An increase in iron was associated with a decrease in Cd volume that in turn accounted for lesser improvement in verbal working memory; however, the complete indirect effect was a non-significant trend.

Whereas Cd iron was indirectly associated with verbal working memory, it was directly associated with lesser improvement in spatial navigation over time. Smaller Cd volumes have been correlated with cross-sectional age-related deficits in vMWM navigation (Moffat et al., 2007). However, here longitudinal iron accumulation and not volumetric shrinkage accounted for differences in spatial navigation efficiency. The benefits of repeated testing on the vMWM task may follow from a procedural learning component, a function that depends on neostriatal circuits (Packard and Knowlton, 2002). Further, in a rodent model of MWM navigation,

interruption of striatal dopamine (see McNamara and Skelton, 1993 for a review) and induced high concentrations of iron (Maaroufi et al., 2009a; 2009b) mimic the iron-related decline in vMWM place navigation reported here. Thus, subcortical iron accumulation may affect cognitive declines either directly due to impaired neurotransmission or indirectly via oxidative stress that promotes volumetric shrinkage. This study offers the first longitudinal evidence for a role of iron accumulation in a nomological model of cognitive aging.

This model of aging includes other correlates of cognitive decline, such as volumetric shrinkage in other regions. Hc volume shrinkage, but not iron accumulation, was associated with a decreased benefit in verbal working memory retest, and not in spatial navigation. Previous cross-sectional study had suggested a mediation effect of increased iron on memory decline through decreased Hc volume (Rodrigue et al., 2012). This was not supported in the longitudinal model. Although a similar cross-sectional association between age, iron, volume, and memory was found at baseline. Cross-sectional studies provide a biased estimate of change, whereas longitudinal study is a more accurate portrayal of the gradual aging process (Lindenberger et al., 2011; Raz and Lindenberger, 2011).

Based on the pattern of longitudinal change reported here, regional iron accumulation appears to precede the volumetric shrinkage and cognitive declines that are hallmarks of aging (Raz et al., 2004; Raz, 2005; Horn and Donaldson, 1980). The accumulation of iron partially accounted for differential associations between age and regional brain volumes that are frequently observed (see Raz et al., 2005). Moreover, baseline iron was associated with subsequent volumetric shrinkage. Thus, high iron content foreshadowed later decline. The utility of iron as a biomarker for neural decline has been suggested (Schenck and Zimmerman, 2004) but until now it had not been tested in a longitudinal study of normal aging.

Establishing non-heme iron as a harbinger of impairment has immediate clinical applications. Whereas other risk factors are systemic and measured peripherally, iron is localized and can be observed directly in the brain (Thomas et al., 1993). Further, iron is easily detectable with MRI using noninvasive methods that can be adapted for clinical diagnostic criteria. MRI screening of iron is a current standard in the diagnosis of neurodegeneration with brain iron accumulation—diseases that are characterized by an extreme concentration of brain iron presenting in early life (see Zecca et al., 2004 for a review). A similar approach to identify adults at a higher risk for declines in aging may be feasible in the future. In addition to improving diagnostic criteria of age-related disease, early detection in normal aging may allow for interventions to help maintain function longer into later life. The predictive validity of iron as a biomarker for future neural and cognitive decline requires additional longitudinal study.

Study Limitations

These findings should be interpreted with consideration of the study limitations. First, T2* is a sensitive, but not specific, measure of iron in the brain, as differences in T2* can be caused by the accumulation of other magnetic materials (Haacke et al., 2005). For example, calcium, which may increase in subcortical regions with age (Naderi et al., 1993), can be distinguished from iron in MRI only with phase-based imaging (Haacke et al., 2005). Future longitudinal studies may benefit from including several iron imaging methods to allow potentially more sensitive and more specific measurements. Validity of T2* as an index of iron content may be threatened by regional differences in myelination (Fukunaga et al., 2010; Langkammer et al., 2012; Lodygensky et al., 2012). Although the influence of myelin in the basal ganglia is likely negligible (Daugherty and Raz, 2013), the T2* measures should be interpreted with this possible confound in mind.

Second, the longitudinal modeling in the larger sample was limited to two measurement occasions. Such pre-post design allows for an accurate estimation of linear change, but potential non-linear effects are obscured (McArdle and Hamagami, 2001). The second sample had additional time points, but due to limitations of sample size, non-linear effects could not be adequately tested. The several null effects in the second sample may reflect the suggested non-linearity in lifespan change approaching a threshold between healthy aging and prodromal disease. The selection for optimal health and limited age range of the second sample may have further minimized the effects that would otherwise be observed in a lifespan sample of more representative health history.

Third, the longitudinal models cannot establish causality amongst factors. The models were constructed based on theory to test for iron accumulation preceding volumetric shrinkage and cognitive declines. These models represented the observed data well. Animal studies of interventions support the model of change in iron preceding volume shrinkage (e.g., Zhang et al., 2009), but the longitudinal models presented here cannot independently establish causality. Several longitudinal time points are necessary to test for temporal precedence and it remains questionable to what extent observational measurements can assess causality at all (Winship and Morgan, 1999; also see Rubin, 2005; Pearl, 2013a, 2013b).

Conclusion

In conclusion, this is the first longitudinal evidence for subcortical accumulation of iron as a factor in cognitive aging. Regional differences in iron suggest a possible metabolic demand that initial increase in iron may be used to meet. However, eventually the excess becomes deleterious. As shown here, an accumulation of iron preceded volumetric shrinkage in the striatum, but not in the Hc or GP. Individual differences in the accumulation of iron and

volumetric shrinkage were partially accounted for by MetS. Persons with high MetS scores had greater iron at baseline that subsequently accounted for volumetric shrinkage. Critically, large iron content at baseline was predictive of subsequent volumetric shrinkage over two years. Finally, increased iron and shrinkage of the Cd was associated with lesser improvement on verbal working memory and spatial navigation tasks. Taken together, high iron content may be a meaningful biomarker of neural and cognitive declines in normal aging.

APPENDIX A

Longitudinal Sample Attrition

Table A1. Detailed description of Sample 1 attrition between baseline and the 2-year follow up.

Reason for Exclusion/Attrition	n
Original Sample	360
Unwilling to participate/Lost Contact	154
Screening Failures/Below Normal Hearing	18
MRI error/MRI incompatibility	83
MRI incidental findings	3
Development of exclusionary conditions at Follow-up (medical diagnosis, CESD, MMSE)	10
Sequence was not collected	3
Retained Sample	89

Table A2. Detailed description of Sample 2 attrition across 4 time points.

Reason for Exclusion/Attrition	Baseline	1 st	2 nd	3 rd
		Follow-up	Follow-up	Follow-up
Original Sample	91	--	--	--
Unwilling to participate/Lost Contact	56		2	10
Screening Failures/Below Normal Hearing	3			
MRI error/MRI incompatibility				1
MRI incidental findings		1		
Development of exclusionary conditions (medical diagnosis, CESD, MMSE)		7	9	9
Deceased				1
Retained Sample	32	32	30	21
Sub-sample of cases that developed exclusionary criteria		8	9	9

APPENDIX B

Detailed description of the manual tracing procedures for each region of interest.

Basal ganglia. The caudate (Cd), putamen (Pt), and globus pallidus (GP) were ranged together. The ventral section began with the first slice on which the head of the caudate appeared, dorsal to visualization of the substantia nigra and red nuclei. Due to the inconsistency in image clarity, the GP and Pt could not be reliably traced ventral to the Cd. The GP ROI included the *pars medialis* and *lateralis* as a single region. The GP and Pt were traced until no longer visualized. The Cd ROI included only the head and body of the caudate, excluding the tail. The Cd range terminated when the lateral thalamic nucleus was no longer visualized, at which point the head and tail of the caudate became continuous. The three ROIs were traced on every slice of the respective range, which was approximately eight slices for the Cd and Pt, and five slices for the GP. The ICC(3) for total volume and average T2*, respectively, was 0.99 and 0.98 for Cd, 0.99 and 0.98 for GP, and 0.99 and 0.97 for Pt.

Hippocampus. The ROI included the head and body of the hippocampus (Hc), excluding the fimbria-fornix; however, the image resolution was not high enough to distinguish subfields of the hippocampus. The most ventral slice began with visualization of the superior colliculus and red nucleus, while the cerebellar vermis were still visualized. The terminal end of the range was marked when the head of the caudate was visualized. The Hc was traced on approximately six contiguous slices. The ICC(3) for total volume and average T2* were 0.99 and 0.95, respectively.

Lamina quadrigemina. The inferior and superior colliculi were traced as a single ROI: the lamina quadrigemina (LQ). The ventral slice was identified by the first visualization of the inferior colliculi when the red nucleus, substantia nigra, and cerebellar vermis were still

visualized. The ROI was traced on four contiguous slices that terminated when the superior colliculi were no longer visualized. The ICC(3) for total volume and average T2* were both 0.98.

APPENDIX C

Longitudinal Latent Model Construction Diagrams

Figure C1. Example simple effects latent change score models for regional volume and iron (T2*). * indicates an estimated parameter; *= indicates an estimated parameter that was constrained across time.

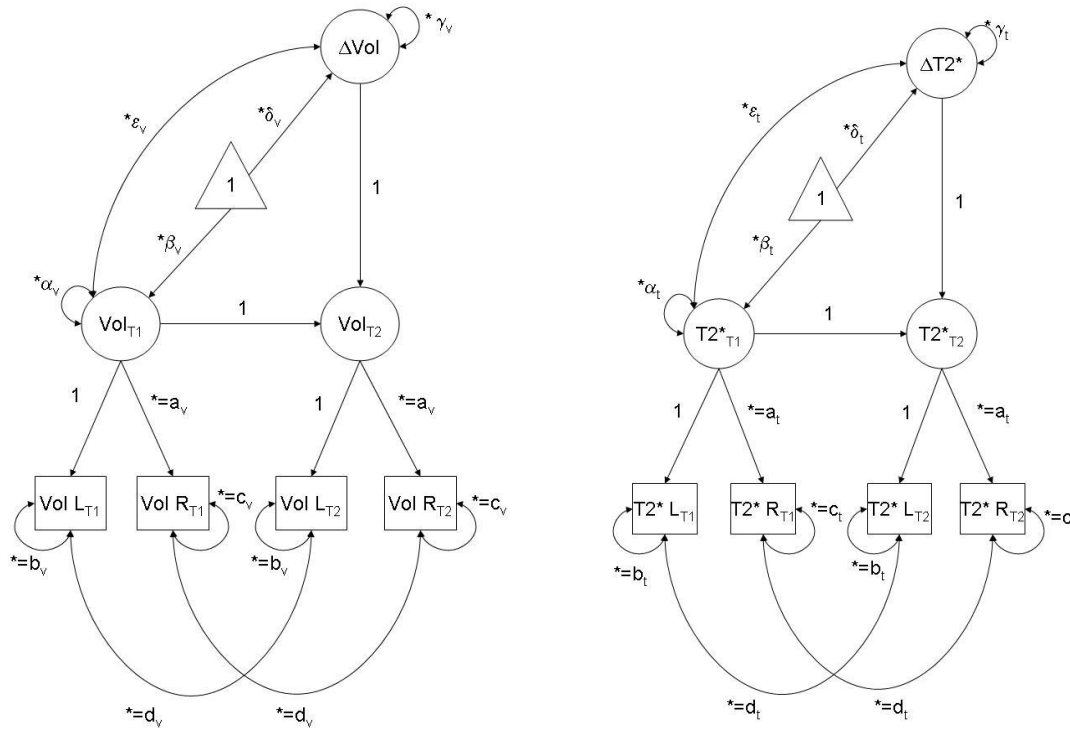


Figure C2. Example simple effects latent change score models for verbal (VWM) and non-verbal working memory (NVWM). * indicates an estimated parameter; *= indicates an estimated parameter that was constrained across time.

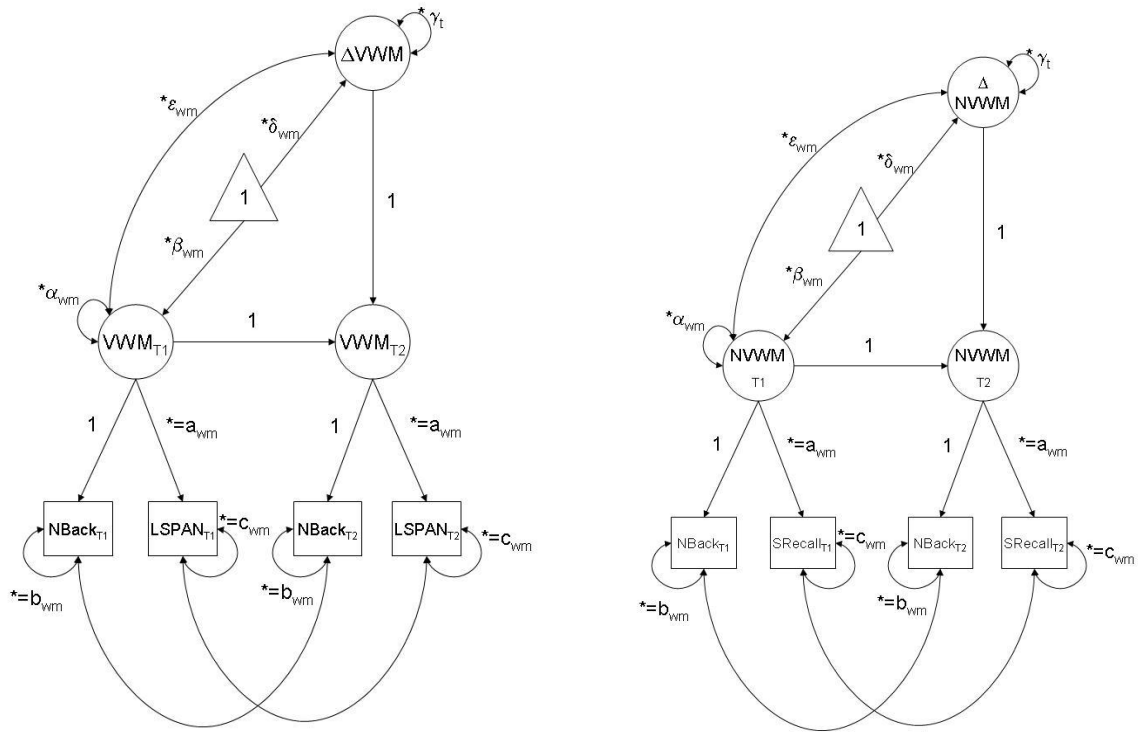


Figure C3. Example simple effects latent change score models for metabolic syndrome (MetS) and inflammation (Inflam). Glu—fasting glucose, HDL—high-density lipoprotein, Triglyc—total triglycerides, HTN—diagnosed or observed hypertension, CRP—C reactive protein, Hcsy—plasma homocysteine, Fol—folate. * indicates an estimated parameter; *= indicates an estimated parameter that was constrained across time.

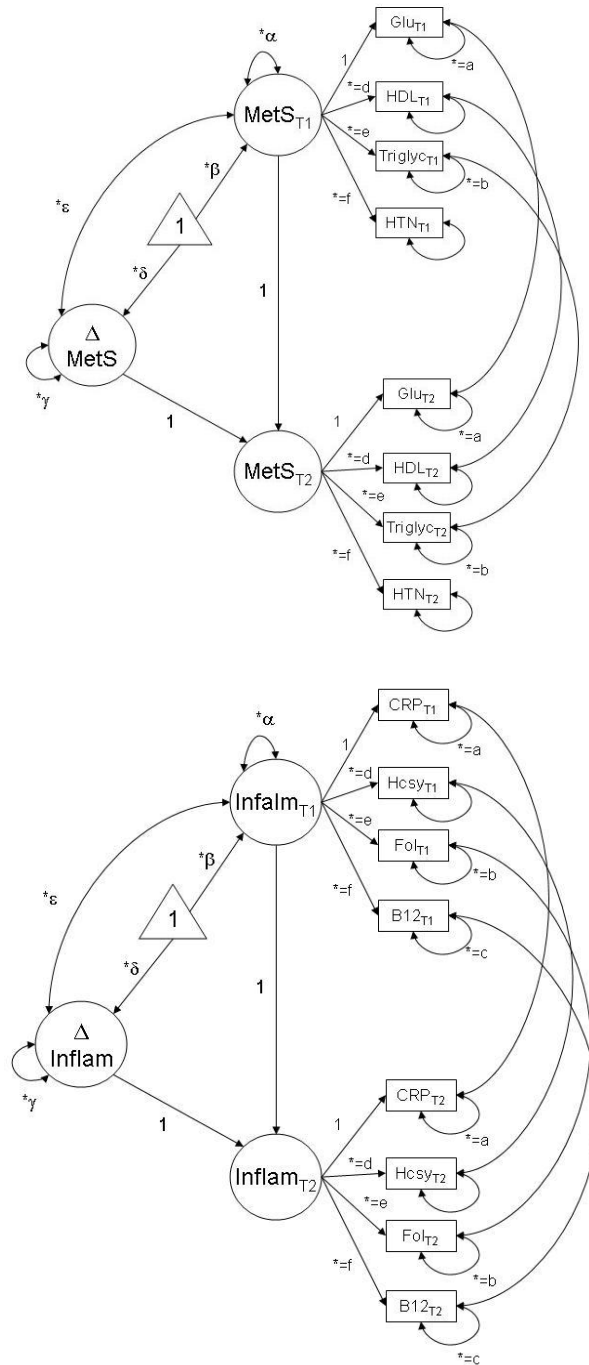


Figure C5. Example of a parallel process model including change in iron, change in volume, change in verbal working memory, and covariates * indicates an estimated parameter; *= indicates an estimated parameter that was constrained across time.

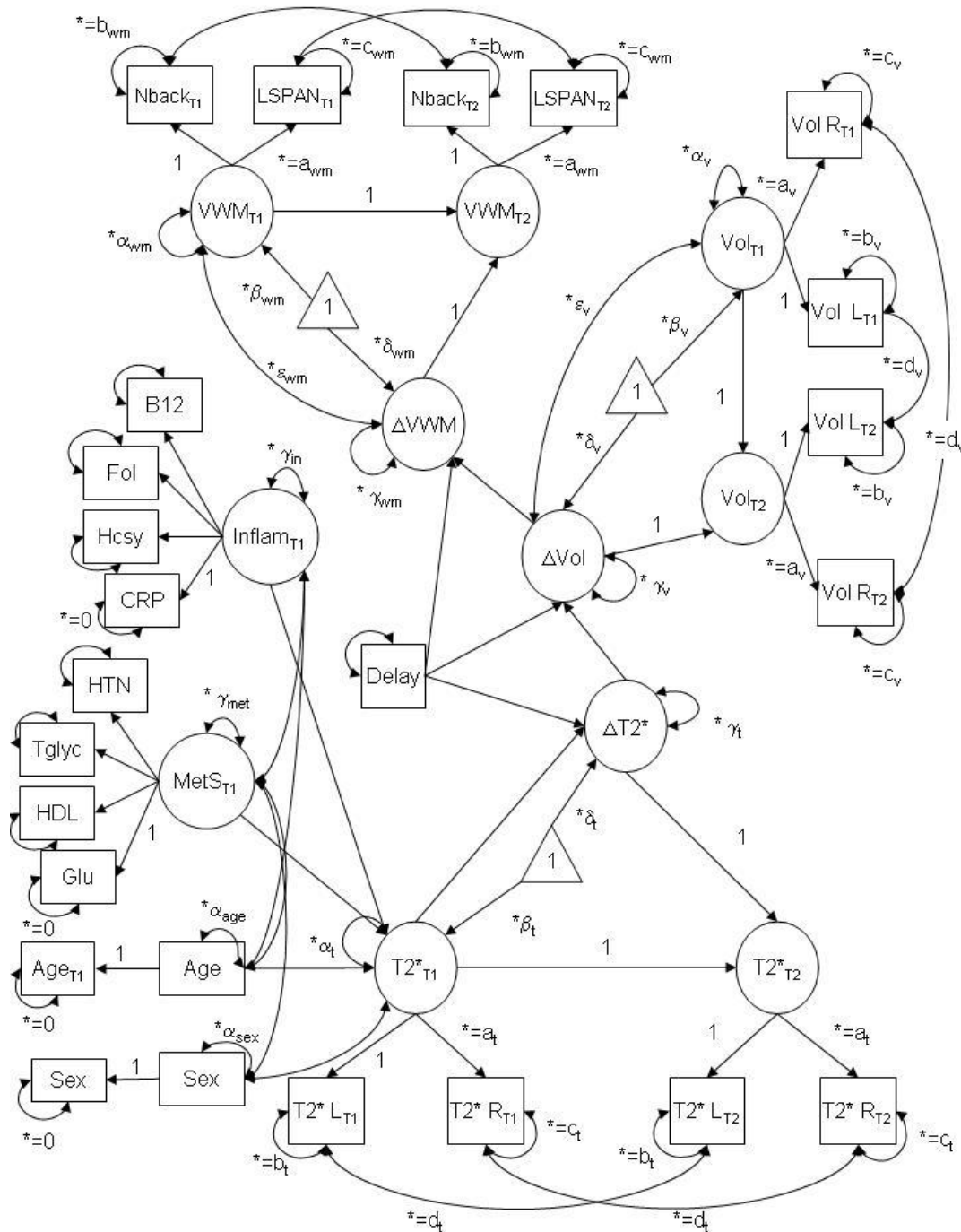


Figure C6. Example of a parallel process model including change in iron, change in volume, change in spatial navigation learning slope, and covariates. * indicates an estimated parameter; *= indicates an estimated parameter that was constrained across time.

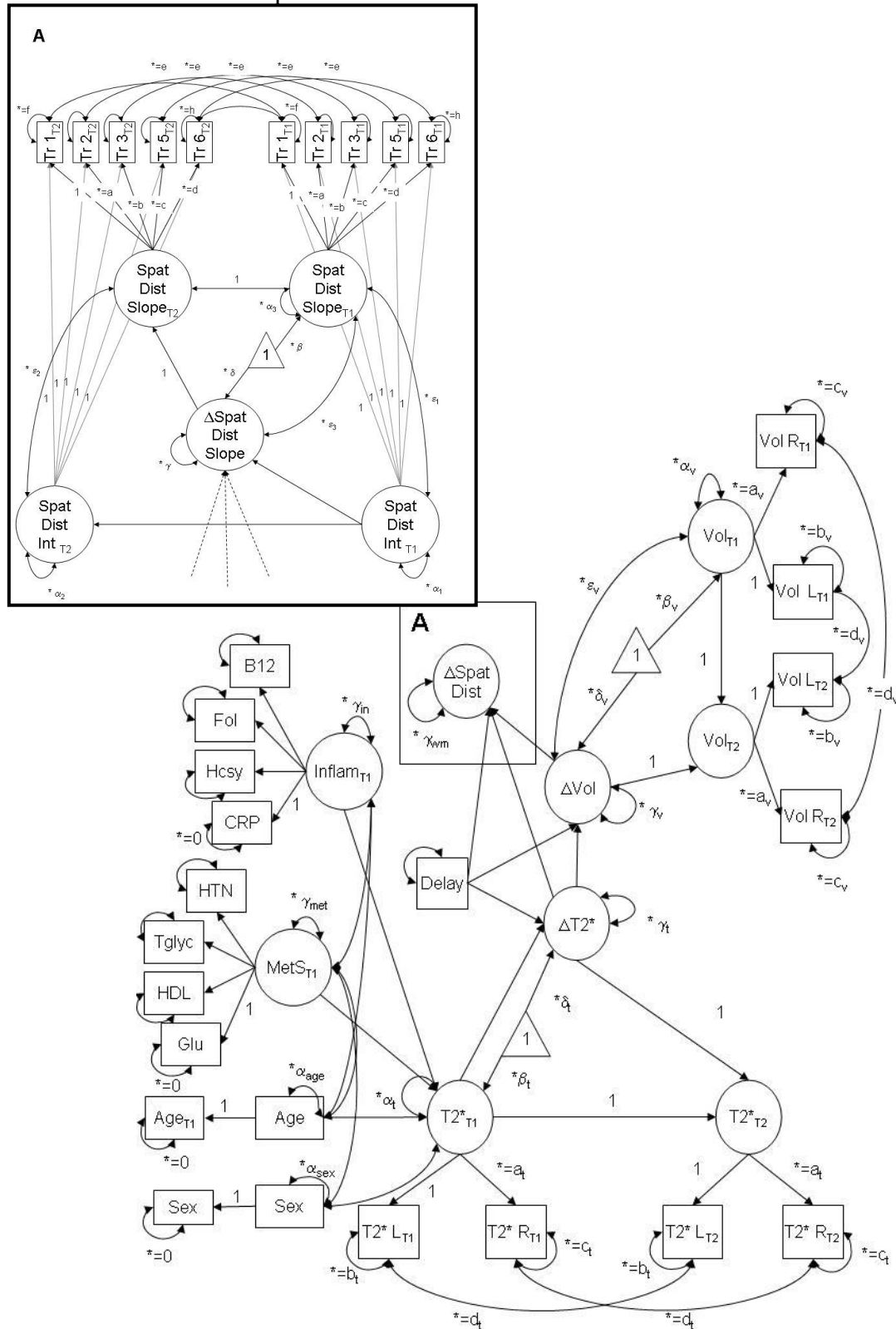


Figure C7. Example of a latent growth curve model for change in volume and iron (T2*). * indicates an estimated parameter; *= indicates an estimated parameter that was constrained across time.

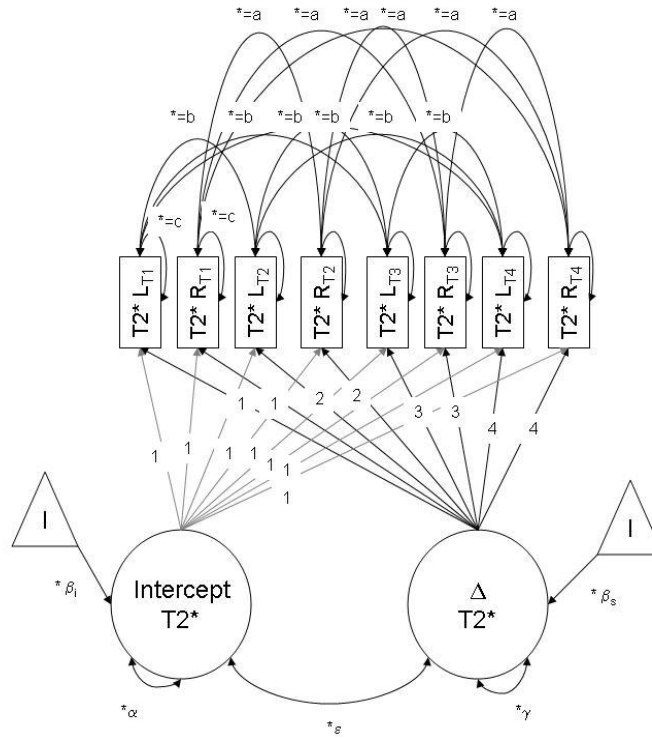
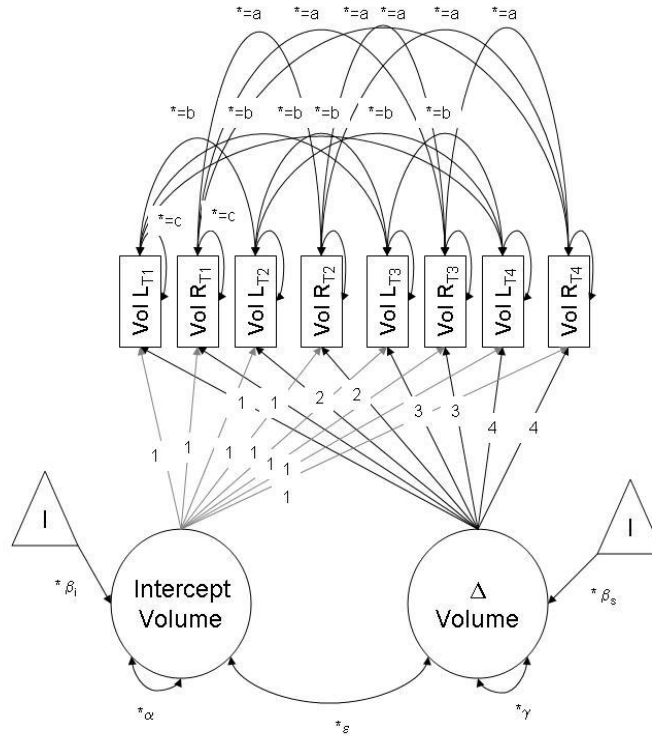
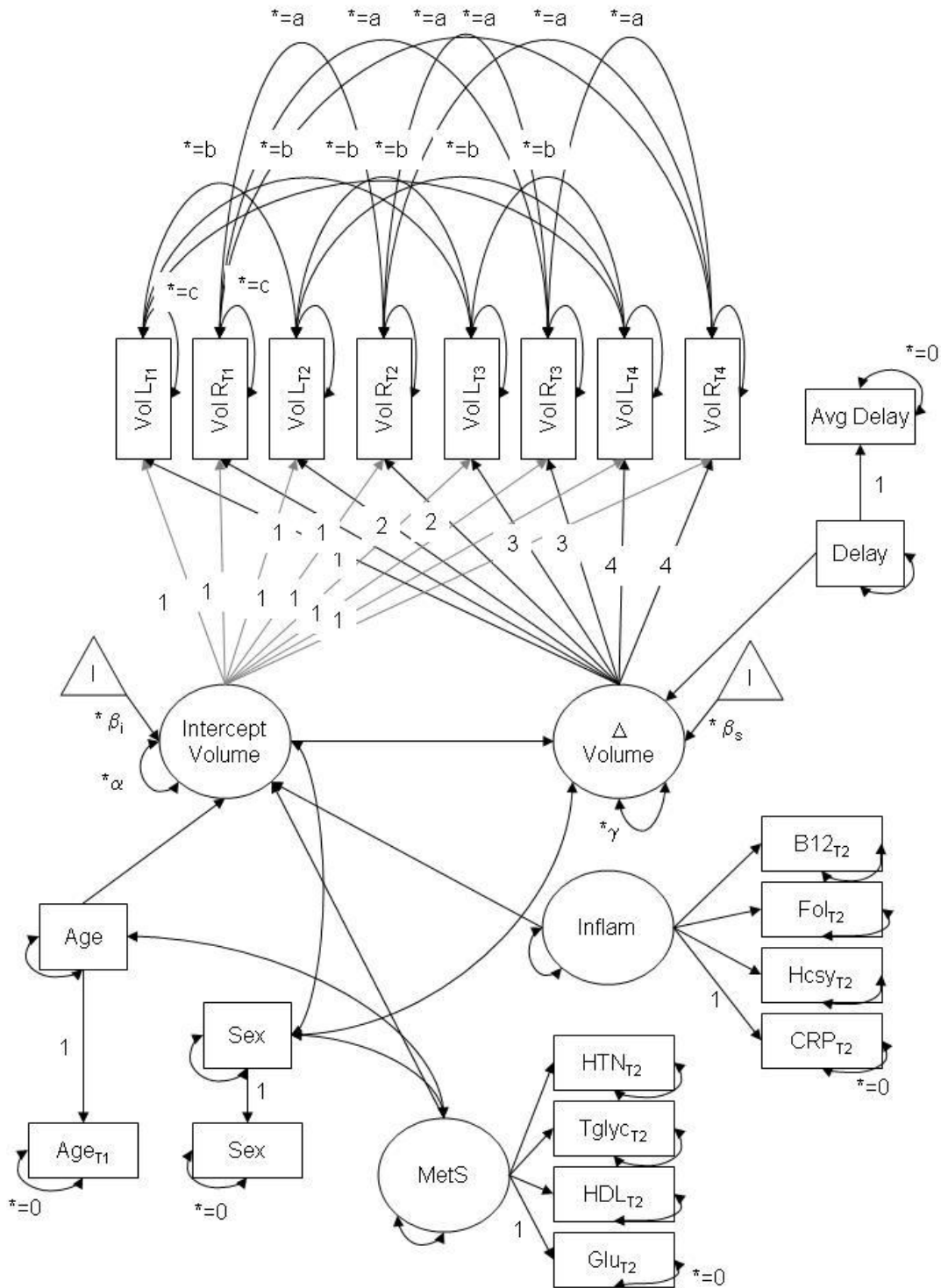


Figure C8. Example of a latent growth curve model including covariates. MetS—metabolic syndrome; Inflammation; Glu—fasting glucose, HDL—high-density lipoprotein, Triglyc—total triglycerides, HTN—diagnosed or observed hypertension, CRP—C reactive protein, Hcsy—plasma homocysteine, Fol—folate.* indicates an estimated parameter; *= indicates an estimated parameter that was constrained across time.



REFERENCES

- Anderson, C.M., Kaufman, M.J., Lowen, S.B., Rohan, M., Renshaw, P.F., & Teicher, M.H. (2005). Brain T2 relaxation times correlate with regional cerebral blood volume. *MGMA*, *181*, 3-6.
- Antonini, A., Leenders, K.L., Meier, D., Oertel, M.D., Boesiger, P., & Anliker, M. (1993). T₂ relaxation time in patients with Parkinson's disease. *Neurol*, *43*, 697-700.
- Ascherio A, Willett WC, Rimm EB, et al. (1994). Dietary iron intake and risk of coronary disease among men. *Circulation*, *89*, 969-74.
- Aquino, D., Bizzi, A., Grisoli, M., Garavaglia, B. *et al.* (2009). Age-related iron deposition in the basal ganglia: quantitative analysis in healthy subjects. *Radiol*, *252(1)*, 165-172.
- Bartzokis, G. (2011). Alzheimer's disease as homeostatic responses to age-related myelin breakdown. *Neurobiol Aging*, *32(8)*, 1341-1371.
- Bartzokis, G., Beckson, M., Hance, D., Marx, P., Foster, J., & Marder, S. (1997). MR evaluation of age-related increase of brain iron in young adult and older normal males. *J Magn Reson Imaging*, *15(1)*, 29-35.
- Bartzokis, G., Cummings, J.L., Markham, C.H., Marmarelis, P.Z. *et al.* (1999). MRI evaluation of brain iron in earlier- and later-onset Parkinson's disease and normal subjects. *J Magn Reson Imaging*, *17(2)*, 213-222.
- Bartzokis, G., Mintz, J., Sultzer, D., Marx, P., Herzberg, J.S., Phelan, C.K., & Marder, S.R. (1994). In vivo MR evaluation of age-related increases in brain iron. *AJNR*, *15(6)*, 1129-1138.
- Bartzokis, G., Sultzer, D., Mintz, J., Holt, L.E., Marx, P., Phelan, C.K., & Marder, S.R. (1994). In vivo evaluation of brain iron in Alzheimer's disease and normal subjects using MRI.

- Biol Psychiatry*, 35, 480-487.
- Bartzokis, G., Lu, P., Tingus, K., Peters, D. *et al.* (2011). Gender and iron genes may modify associations between brain iron and memory in healthy aging. *Neuropsychopharmacology*, 36, 1375-1384.
- Bartzokis, G., Lu, P.H., Tishler, T., Peters, D. *et al.* (2010). Prevalent iron metabolism gene variants associated with increased brain ferritin iron in healthy older men. *JAD*, 20, 333-341.
- Bartzokis, G., Tishler, T.A., Lu, P.H., *et al.* (2007). Brain ferritin iron may influence age- and gender-related risks of neurodegeneration. *Neurobiol Aging*, 28, 414-423.
- Berg, D., Kruger, R., RieB, R., & Riederer, P. (2007). Parkinson's disease. In: M. Youdim, P. Riederer, S. Mandel, and L. Battistin (Eds.). *Handbook of Neurochemistry and Molecular Neurobiology: Degenerative Diseases of the Nervous System (3rd Ed.)*, pp 1-20. Springer: New York, NY.
- Berry, C., Brosnan, M.J., Fennel, J., Hamilton, C.A., & Dominiczak, A.F. (2001). Oxidative stress and vascular damage in hypertension. *Current opinion in Nephrology and Hypertension*, 10(2), 247-255.
- Bilgic, B., Pfefferbuam, A., Rohlfing, T., Sullivan, E., & Adalsteinsson, E. (2011). MRI estimates of brain iron concentration in normal aging using quantitative susceptibility mapping. *NeuroImage*, 59(3), 2625-2635.
- Bizzi, A., Brooks, R.A., Brunetti, A., *et al.* (1990). Role of iron and ferritin in MR imaging of the brain: A study in primates at different field strengths. *Radiol*, 177, 59-65.
- Bloch, B., Popocivi, T., Levin, M.J., Tuil, D., & Kahn, A. (1985). Transferrin gene expression visualized in oligodendrocytes of a rat brain by using in situ hybridization and

- immunohistochemistry. *Proc Nat Acad Sci USA*, 82, 6706-10.
- Brass, S.D., Chen, N., Mulkern, R., & Baksni, R. (2006). Magnetic resonance imaging of iron deposition in neurological disorders. *Top Magn Reson Imaging*, 17(1), 31-40.
- Cabantchik, Z.I., Kakhlon, O., Epsztejn, S., Zanninelli, G., & Breuer, W. (2002). Intracellular and extracellular labile iron pools. *Adv Exp Med Biol*, 509, 55-75.
- Cherubini, A., Peran, P., Caltagirone, C., Sabatini, U., & Spalletta, G. (2009). Aging of subcortical nuclei: Microstructural, mineralization and atrophy modifications measured in vivo using MRI. *NeuroImage*, 48, 29-36.
- Crichton, R.R. and Ward, R.J. Structure and molecular biology of iron and iron-binding proteins. In: Lauffer (Ed.) *Iron and Human Disease*, pp 365-394. CRC Press: Boca Baton, FL.
- Dahle, C., Jacobs, B., & Raz, N. (2009). Aging, vascular risk and cognition: Blood glucose, pulse pressure, & cognitive performance in healthy adults. *Psychology of Aging*, 24(1), 154-162.
- Daugherty, A. & Raz, N. (2013). Age-related differences in iron content of subcortical nuclei observed in vivo: A meta-analysis. *NeuroImage*, 70, 113-121.
- Daugherty, A.M., Yuan, P., Dahle, C.L., Bender, A.R., Yang, Y., & Raz, N. (2014). Path complexity in virtual water maze navigation: Differential associations with age, sex, and regional brain volume. *Cerebral Cortex*. [Epub ahead of print].
- Deane, R., Zheng, W., & Zlokovic, B.V. (2004). Brain capillary endothelium and choroid plexus epithelium regulate transport of transferrin-bound and free iron into the rat brain. *Journal of Neurochemistry*, 88, 813-820.

- Diezel, P.B. (1955). Iron in the brain: A chemical and histochemical examination. In H. Waelsch (Ed.), *Biochemistry of the Developing Nervous System*, p. 145ff. New York, NY: Academic Press, Inc.
- Ding, B., Chen, K.-M., L., J.-W., Sun, F. *et al.* (2009). Correlation of iron in the hippocampus with MMSE in patients with Alzheimer's disease. *Journal of Magnetic Resonance Imaging*, 29, 793-798.
- Dobbs, A.R., & Rule, B.G. (1989). Adult age differences in working memory. *Psychology and aging*, 4, 500-503.
- Dong, X.P., Cheng, X., Mills, E., Delling, M., Wang, F., Kurz, T., & Xu, H. (2008). The type IV mucopolidosis-associated protein TRPML1 is an endolysosomal iron release channel. *Nature*, 455(7215), 992-996.
- Drayer, B. (1988). Imaging of the aging brain: Part I. normal findings. *Radiol*, 166, 785-796.
- Duvernoy, H.M. (1988). *The Human Hippocampus: An Atlas of Applied Anatomy*. Springer: New York, NY.
- Duvernoy, H.M. (1999). *Human Brain Stem Vessels: Including the Pineal Gland and Information on Brain Stem Infarction*. Springer: New York, NY.
- Engle, R.W., Cantor, J., & Carullo, J. (1992). Individual differences in working memory and comprehension: A test of four hypotheses. *Journal of experimental Psychology: Learning, Memory and Cognition*, 18, 972-992.
- Feekes, J.A. and Cassell, M.D. (2006). The vascular supply of the functional compartments of the human striatum *Brain*, 129, 2189-2201.
- Fernandez-Real JM, Lopez-Bermejo A, Ricart W. (2005). Iron stores, blood donation, & insulin sensitivity and secretion. *Clin Chem*, 51, 1201-5.

- Fisher, J., Ingram, D., Slagle-Webb, B., Madhankumar, A.B. *et al.* (2006). Ferritin: a novel mechanism for delivery of iron to the brain and other organs. *Am J Cell Physiol*, 293, C641-C649.
- Folstein, M.F., Folstein, S.E., & McHugh, P.R. (1975). "Mini-mental state". A practical method for grading the cognitive state of patients for the clinician. *Journal of Psychiatric Research*, 12, 189-198.
- Fratiglioni, L. & Wang, H.X. (2007). Brain reserve hypothesis in dementia. *Journal of Alzheimer's disease*, 12(1), 11-22.
- Fukunaga M, Li TQ, van Gelderen P, de Zwart JA, Shmueli K, Yao B, Lee J, Maric D, Aronova MA, Zhang G, Leapman RD, Schenck JF, Merkle H, Duyn JH. (2010). Layer-specific variation of iron content in cerebral cortex as a source of MRI contrast. *Proc Natl Acad Sci U S A*, 107, 3834-3839.
- Gomori, J. & Grossman, R. (1993). The relation between regional brain iron and T2 shortening. *AJNR*, 14, 1049-1050.
- Grundy, S.M., Cleeman, J.I., Daniels, S.R., Donato, K.A., et al. (2005). Diagnosis and management of the metabolic syndrome: An American Heart Association/National Heart, Lung, and Blood Institute scientific statement. *Circulation*, 112, 2735-2752.
- Gunshin, H., Mackenzie, B., Berger, U.V., Gunshin, Y. *et al.* (1997). Cloning and characterization of a mammalian proton-coupled metal-ion transporter. *Nature*, 388, 482-488.
- Haacke, E.M., Ayaz, M., Khan, A., Manova, E.S., *et al.* (2007). Establishing a baseline phase behavior in magnetic resonance imaging to determine normal vs. abnormal iron content in the brain. *Journal of Magnetic Resonance Imaging*, 26(2), 256-264.

- Haacke, E.M., Cheng, N.Y.C., House, M.J., *et al.* (2005). Imaging iron stores in the brain using magnetic resonance imaging. *J Magn Reson Imaging*, 23(1), 1-25.
- Haacke, E.M., Miao, Y., Liu, M., Habib, C.A., Katkuri, Y., Liu, T., Yang, Z., Lang, Z., Hu, J., & Wu, J. (2010). Correlation of putative iron content as represented by changes in R2 and phase with age in deep gray matter of healthy adults. *J Magn Reson Imaging*, 32, 561-576.
- Hallervorden, J. and Spatz, H. (1922). Peculiar disease of the extrapyramidal system with particular affection of the globus pallidus and the substantia nigra. (Translation). *Z. Ges. Neurol Psychiat*, 79, 254-302.
- Hallgren, B. and Sourander, P. (1958). The effect of age on the non-haemin iron in the human brain. *J Neurochem*, 3, 41-51.
- Halliwell, B. (1992). Iron and damage to biomolecules. In: Lauffer (Ed.) *Iron and Human Disease*, pp 209-236. CRC Press: Boca Raton, FL.
- Hamilton, M.L., Van Remmen, H., Drake, J., Yang, H. *et al.* (2001). Does oxidative damage to DNA increase with age? *PNAS*, 98(18), 10469-10474.
- Harder, S.L., Hopp, K.M., Ward, H., Neglio, H., Gitlin, J., & Kido, D. (2008). Mineralization of the deep gray matter with age: A retrospective review with susceptibility-weighted MR imaging. *AJNR*, 29, 176-183.
- Hare, D., Ayton, S., Bush, A., & Lei, P. (2013). A delicate balance: Iron metabolism and diseases of the brain. *Frontiers in Aging Neuroscience*, 5, 34.
- Hare, D.J., Lee, J.K., Beavis, A.D., van Gramberg, A., George, J., Adlard, P.A., Finkelstein, D.I., & Doble, P.A. (2012). Three-dimensional atlas of iron, copper, and zinc in the mouse cerebrum and brainstem. *Anal Chem*, 84, 3990-3997.

- Harman, D. (1956). Aging: A theory based on free radical and radiation chemistry. *J Gerontol*, *11*(3), 298-300.
- Hasan, K.M., Halphen, C., Boska, M.D., & Narayana, P.A. (2008). Diffusion tensor metrics, T₂ relaxation, and volumetry of the naturally aging human caudate nuclei in healthy young and middle-aged adults: possible implications for the neurobiology of human brain aging and disease. *Magn Reson Med*, *59*, 7-13.
- Hasan, K.M., Halphen, C., Kamali, A., Nelson, F.M., Wolinsky, J.S., & Narayana, P.A. (2009). Caudate nuclei volume, diffusion tensor metrics, and T₂ relaxation in healthy adults and relapsing-remitting multiple sclerosis patients: Implications to understanding gray matter degeneration. *J Magn Reson Imaging*, *29*(1), 70-77.
- Hawker, K. & Lang, A.E. (1990). Hypoxic-ischemic damage of the basal ganglia. Case reports and a review of the literature. *Movement Disorders*, *5*(3), 219-224.
- Hayes, A.F. and Scharkow, M. (2013). The relative trustworthiness of inferential tests of the indirect effect in statistical mediation analysis: Does method really matter? *Assoc Psych Sci*. [Epub ahead of print].
- Head, D., Raz, N., Gunning-Dixon, F., Williamson, A., & Acker, J.D. (2002). Age-related shrinkage of the prefrontal cortex is associated with executive, but not procedural aspects of cognitive performance. *Psychology and Aging*, *17*, 72-84.
- Hertzog, C., Dixon, R.A., & Hultsch, D.F. (1992). Intraindividual change in text recall of the elderly. *Brain and Language*, *42*, 248-269.
- Hill, J.M. & Switzer, R.C. (1984). The regional distribution and cellular localization of iron in the rat brain. *Neuroscience*, *11*(3), 595-603.
- Hirai, W., Korogi, Y., Sakamoto, Y., Hamatake, S., Ikushima, I., & Takahashi, M. (1996). T₂

- shortening in the motor cortex: Effect of aging and cerebrovascular diseases. *Radiology*, 199, 799-803.
- Horn, J.L. & Donaldson, G. (1980). Cognitive development in adulthood. In O.G. Brim, Jr. & J. Kagan (eds.). *Constancy and change in human development*, pp 445-529. Cambridge, MA: Harvard University Press.
- House, E., Collingwood, J., Khan, A., Korchazkina, O., Berthon, G., & Exley, C. (2004). Aluminum, iron, zinc and copper influence the in vitro formation of amyloid fibrils of Abeta42 in a manner which may have consequences for metal chelation therapy in Alzheimer's disease. *J Alz Dis*, 6(3), 291-301.
- Jack, Jr, C.R., Twomey, C.K., Zinsmeister, A.R., Sharbrough, F.W., Petersen, R.C., Cascino, G.D. (1989). Anterior temporal lobes and hippocampal formations: normative volumetric measurements from MR images in young adults. *Radiology*, 172, 549-554.
- James, L.R. & Brett, J.M. (1984). Mediators, moderators, and tests for mediation. *Journal of Applied Psychology*, 69, 307-321.
- Jara, H., Sakai, O., Mankal, P., Irving, R., & Norbash, A. (2006). Multispectral quantitative magnetic resonance imaging of brain iron stores: a theoretical perspective. *Top Magn Reson Imaging*, 17, 19-30.
- Jehn M, Clark JM, Guallar E. (2004). Serum ferritin and risk of the metabolic syndrome in U.S. adults. *Diabetes Care*, 27, 2422-8.
- Joseph, J.A., Shukitt-Hale, B., Casadesus, G., & Fisher, D. (2005). Oxidative stress and inflammation in brain aging: Nutritional considerations. *Neurochem Res*, 30(6/7), 927-935.
- Kado, D.M., Karlamangla, A.S., Huang, M.H., Troen, A., Rowe, J.W., Selhub, J., & Seeman,

- T.E. (2005). Homocysteine versus vitamins folate, B6, and B12 as predictors of cognitive function and decline in older high-functioning adults: MacArthur studies of successful aging. *American Journal of Medicine*, 118(2), 161-7.
- Kroll, J.f. & Potter, M.C. (1984). Recognizing words, pictures and concepts: A comparison of lexical, object and reality decisions. *Journal of Verbal Learning and Verbal Behavior*, 23, 39-66.
- Kumar, R., Delshad, S., Woo, M.A., Macey, P.M., & Harper, R.M. (2011). Age-related regional brain T2-relaxation changes in healthy adults. *J Magn Reson Imaging*, 35(2), 300-308.
- Langkammer, C., Krebs, N., Goessler, W., Scheurer, E., Yen, K., Fazekas, F., & Ropele, S. (2012). Susceptibility induced gray-white matter MRI contrast in the human brain. *NeuroImage*, 59, 1413-1419.
- Larsen, R. (2011). Missing data imputation versus full information maximum likelihood with second-level dependencies. *Structural Equation Modeling: A Multidisciplinary Journal*, 18(4), 649-662.
- Lauffer, R. (Ed.). (1992). Introduction. Iron, aging, and human disease: Historical background and new hypotheses. In: *Iron and Human Disease*, pp 1-22. CRC Press: Boca Raton, FL.
- Lindenberger, U., Mayr, U., & Kliegl, R. (1993). Speed and intelligence in old age. *Psychology and Aging*, 8, 207-220.
- Lindenberger, U., von Oertzen, T., Ghisletta, P., & Hertzog, C. (2011). Cross-sectional age variance extraction: What's change got to do with it? *Psychol Aging*, 26, 34-47.
- Lodygensky, G.A., Marques, J.P., Maddage, R., Perroud, E., Sizonenko, S.V., Hüppi, P.S., & Gruetter, R. (2012). In vivo assessment of myelination by phase imaging at high

- magnetic field. *NeuroImage*, 59, 1979-1987.
- Loitfelder, M., Seiler, S., Schwingenschuh, P., & Schmidt, R. (2012). Cerebral microbleeds: a review. *Panminerva Med*, 54, 149-160.
- Maaroufi, K., Ammari, M., Jeljeli, M., Roy, V., Sakly, M., & Abdelmelek, H. (2009a). Impairment of emotional behavior and spatial learning in adult Wistar rats by ferrous sulfate. *Physiology and Behavior*, 96, 343-349.
- Maaroufi, K., Had-Aissouni, L., Melon, C., Sakly, M., Abdelmelek, H., Poucet, B., & Save, E. (2009b). Effects of prolonged iron overload and low frequency electromagnetic exposure on spatial learning and memory in the young rat. *Neurobiology of Learning and Memory*, 92, 345-355.
- Mallikarjun, V., Sriram, A., Scialo, F., & Sanz, A. (2014). The interplay between mitochondrial protein and iron homeostasis and its possible role in aging. *Experimental Gerontology*. [Epub ahead of print].
- Martin, W.R.W., Ye, F.Q., & Allen, P.S. (1998). Increasing striatal iron content associated with normal aging. *Mov Disord*, 13(2), 281-286.
- Mattson, M.P. and Shea, T.B. (2003). Folate and homocysteine metabolism in neural plasticity and neurodegenerative disorders. *TRENDS in Neuroscience*, 26(3), 137-146.
- Maxwell, S.E. & Cole, D.A. (2007). Bias in cross-sectional analyses of longitudinal mediation. *Psychol Methods*, 12(1), 23-44.
- McArdle, J.J. & Hamagami, F. (2001). Latent difference score structural models for linear dynamic analyses with incomplete longitudinal data. In L.M. Collins & A.G. Sayer, *New Methods for the Analysis of Change. Decade of Behavior*, pp. 139-175. APA: Washinton, D.C.

- McNamara, R.K. & Skelton, R.W. (1993). The neuropharmacological and neurochemical basis of place learning in the Morris water maze. *Brain Research Reviews*, 18(1), 33-49.
- Mills, E., Dong, X., Wang, F., & Xu, H. (2010). Mechanisms of brain iron transport: Insight into neurodegeneration and CNS disorders. *Future Med Chem*, 2(1), 51-72.
- Moffat, S.D. (2009). Aging and spatial navigation: What do we know and where do we go? *Neuropsychol Rev*, 19, 478-489.
- Moffat SD, Kennedy K, Rodrigue K, Raz N. 2007. Extra-hippocampal contributions to age differences in human spatial navigation. *Cereb Cort*. 17(6): 1274-1282.
- Moffat SD, Resnick SM. 2002. Effects of age on virtual environment place navigation and allocentric cognitive mapping. *Behav Neurosci*. 116(5): 851-859.
- Moos, T. and Morgan, E.H. (2004). The metabolism of neuronal iron and its pathogenic role in neurologic disease: review. *Ann N Y Acad Sci*, 1012, 14-26.
- Moos, T., Rosengren Nielsen, T., Skjorringe, T., & Morgan, E.H. (2007). Iron trafficking inside the brain. *J Neurochem*, 103(5), 1730-1740.
- Muthen, B., Kaplan, D., & Hollis, M. (1987). On structural equation modeling with data that are not missing completely at random. *Psychometrika*, 52, 431-462.
- Naderi, S., Colakoglu, Z., Luleci, G. (1993). Calcification of basal ganglia associated with pontine calcification in four cases: A radiologic and genetic study. *Clin Neurol Neurosurg*, 95(2), 155-157.
- Nams, V.O. (2006). Improving accuracy and precision in estimating fractal dimension of animal movement paths. *Acta Biotheoretica*, 54, 1-11.
- Oldfield, R.C. (1971). The assessment and analysis of handedness. *Neuropsychologica*, 9, 97-113.

- Packard, M.G. and Knowlton, B.J. (2002). Learning and memory functions of the basal ganglia. *Annu Rev Neurosci*, 25, 563-593.
- Park, D.C. (2000). The basic mechanism accounting for age-related decline in cognitive function. In D.C. Park and N. Schwarz (Eds.), *Cognitive Aging: A Primer*. Philadelphia: Psychology Press.
- Pearl, J. (2013a). Interpretation and identification of causal mediation. *Psychological Methods*. [Epub ahead of print].
- Pearl, J. (2013b). Reply to commentary by Imai, Keele, Tingley, and Yamamoto, concerning causal mediation analysis. *Psychological Methods*. [Epub ahead of print].
- Petersen, R.C., Smith, G.E., Waring, S.C., et al. (1999). Mild cognitive impairment: clinical characterization and outcome. *Arch Neurol*, 56, 303-308.
- Petersen, R.C., Stevens, J.C., Ganguli, M., Tangalos, E.G., Cummings, J.L., & DeKosky, S.T. (2001). Practice parameter: Early detection of dementia: Mild cognitive impairment (an evidence-based review: Report of the quality standards subcommittee of the American Academy of Neurology. *Neurol*, 56, 1133.
- Petito CK, Pulsinelli WA. 1984. Delayed neuronal recovery and neuronal death in rat hippocampus following severe cerebral ischemia: Possible relationship to abnormalities in neuronal processes. *Journal of Cerebral Blood Flow and Metabolism*, 4(2): 194-205.
- Peran, P., Cherubini, A., Luccichenti, G., et al. (2009). Volume and iron content in the basal ganglia and thalamus. *Hum Brain Mapp*, 30, 2667-2675.
- Peran, P., Hagberg, G., Luccichenti, G., et al. (2007). Voxel-based analysis of R2maps in the healthy human brain. *J Magn Reson Imaging*, 26, 1413-1420.
- Pfefferbaum, A., Adalsteinsson, E., Rohfling, T., & Sullivan, E.V. (2009). MRI estimates of

- brain iron concentration in normal aging: Comparison of field-dependent (FDRI) and phase (SWI) methods. *NeuroImage*, 47(2), 493-500.
- Pfefferbaum, A., Adalsteinsson, E., Rohlfing, T., & Sullivan, E.V. (2010). Diffusion tensor imaging of deep gray matter brain structures: Effects of age and iron concentration. *Neurobiol Aging*, 31(3), 482-500.
- Preacher, K.J., Wichman, A.L., MacCallum, R.C., & Briggs, N.E. (2008). *Latent Growth Curve Modeling*. SAGE Publications, Inc: Thousand Oaks, CA.
- Pujol, J., Junque, C., Vendrell, P., *et al.* (1992). Biological significance of iron-related magnetic resonance imaging changes in the brain. *Arch Neurol*, 49(7), 711-717.
- Pulsinelli WA, Waldman S, Rawlinson D, Plum F. 1982. Moderate hyperglycemia augments ischemic brain damage: A neuropathologic study in the rat. *Neurology*, 32(11): 1239-1246.
- Qin, Y., Zhu, W., Zhan, C., Zhao, L. *et al.* (2011). Investigation on positive correlation of increased brain iron deposition with cognitive impairment in Alzheimer disease by using quantitative MR R2 mapping. *J Huazhong Univ Sci Technol [Med Sci]*, 31(4), 578-585.
- Quintana, C., Bellefqih, S., Laval, J.Y., *et al.* (2006). Study of the localization of iron, ferritin, and hemosedrin in Alzheimer's disease hippocampus by analytical microscopy at the subcellular level. *J Struct Biol*, 153, 42-54.
- Radloff, L.S. (1977). The CES-D scale: A self-report depression scale for research in the general population. *Journal of Structural Biology*, 153, 42-54.
- Raykov, T. & Marcoulides, G.A. (2006). *A first course in structural equation modeling (2nd Ed.)*. Lawrence Erlbaum: Mahwah, NJ.
- Raz, N. (2004). The aging brain observed in vivo: Differential changes and their modifiers. In:

- R. Cabeza , L. Nyberg, & D.C. Park (Eds.). *Cognitive Neuroscience of Aging: Linking Cognitive and Cerebral Aging*, pp 17-55. Oxford University Press: New York, NY.
- Raz, N. (2005). Ageing and the brain. *Encyclopedia of Life Sciences*. John Wiley & Sons, Ltd.: Hoboken, New Jersey.
- Raz, N., Ghisletta, P., Rodrigue, K., Kennedy, K., & Lindenberger, U. (2010). Trajectories of brain aging in middle-age and older adults: Regional and individual differences. *NeuroImage*, *51*(2), 501-511.
- Raz, N. and Kennedy, K.M. (2009). A systems approach to the aging brain: Neuroanatomic changes, their modifiers, and cognitive correlates. In Jagust, W. & D'Esposito, M. (Eds). *Imaging the Aging Brain*, pp. 43-70. Oxford University Press.
- Raz, N. and Lindenberger, U. (2011). Only time will tell: Cross-sectional studies offer no solution to the age-brain-cognition triangle: comment on Salthouse (2011). *Psychol Bull*, *137*(5), 790-795.
- Raz, N., Lindenberger, U., Rodrigue, K.M., *et al.* (2005). Regional brain changes in aging healthy adults : General trends, individual differences, and modifiers. *Cerebral Cortex*, *15*, 1676-1689.
- Raz, N., Rodrigue, K.M., & Haacke, E.M. (2007). Brain aging and its modifiers: Insights from in vivo neuromorphometry and susceptibility weighted imaging. *Annals of the New York Academy of Sciences*, *1097*, 84-93.
- Raz, N., Rodrigue, K. Head, D., Kennedy, K., & Acker, J. (2004). Differential aging of the medial temporal lobe: A study of a five-year change.
- Rice, M.E., Patel, J.C., & Cragg, S.J. (2011). Dopamine release in the basal ganglia. *Neuroscience*, *198*, 112-137.

- Rival, T., Page, R.M., Chandraratna, D.S., *et al.* (2009). Fenton chemistry and oxidative stress mediate the toxicity of the *B*-amyloid peptide in a *Drosophila* model of Alzheimer's disease. *Eur J Neurosci*, *29*, 1335-1347.
- Rodrigue, K.M., Haacke, E.M., & Raz, N. (2011). Differential effects of age and history of hypertension on regional brain volumes and iron. *NeuroImage*, *54*, 750-759.
- Rodrigue, K.M., Daugherty, A.M., Haacke, E.M., & Raz, N. (2012). The role of hippocampal iron concentration and hippocampal volume in age-related differences in memory performance, *Cereb Cortex*.
- Rombouts, S., Scheltens, P., Kuijter, J., & Barkhof, F. (2007). Whole brain analysis of T2* weighted baseline FMRI signal in dementia. *Human Brain Mapping*, *28*, 1313-1317.
- Rubin, D. (2005). Causal inference using potential outcomes: Design, modeling, decisions. *Journal of American Statistical Association*, *100*, 322-331.
- Salthouse, T.A. (1994). The nature of the influence of speed on adult age differences in cognition. *Developmental Psychology*, *30*, 240-259.
- Salthouse, T.A., Hancock, H.E., Meinz, E.J., & Hambrick, D.Z. (1996). Interrelations of age, visual acuity, and cognitive functioning. *Journal of Gerontology: Psychological Sciences*, *51B*, 317-330.
- Salthouse, T.A., Mitchell, D.R.D., Skovronek, e., & Babcock, R.L. (1989). Effects of adult age and working memory on reasoning and spatial abilities. *Journal of Experimental Psychology: Learning, Memory and Cognition*, *15*, 507-516.
- Satz, P. (1993). Brain reserve capacity on symptom onset after brain injury: A formulation and review of evidence for threshold theory. *Neuropsychology*, *7*, 273-295.
- Schenck, J. (1995). Imaging of brain iron by magnetic resonance: T2 relaxation at different field

- strengths. *J Neurol Sci*, 134 (Suppl.), 10-18.
- Schenck, J.F. and Zimmerman, E.A. (2004). High-field magnetic resonance imaging of brain iron: birth of a biomarker? *NMR Biomed*, 17(7), 433-45.
- Schenker, C., Meier, D., Wichmann, W., Boesiger, P., & Valavanis, A. (1993). Age distribution and iron dependency of the T2 relaxation time in the globus pallidus and putamen. *Neuroradiol*, 35, 119-124.
- Shi, Z., Hu, X., Yuan, B., Pan, X., Meyer, H.E., & Holmboe-Ottesen, G. (2006). Association between serum ferritin, hemoglobin, iron intake, and diabetes in adults in Jiangsu, China. *Diabetes Care*, 29(8), 1878-83.
- Shrout, P.E. & Fleiss, J.L. (1979). Intraclass correlations: Uses in assessing raters reliability. *Psychological Bulletin*, 86, 420-428.
- Siemonsen, S., Finsterbusch, J., Matschke, J., Loernzen, A., Ding, X.-Q., & Fiehler, J. (2008). Age-dependent normal values of T2 and T2' in brain parenchyma. *Am J Neuroradiol*, 29, 950-955.
- Singh, A., Isaac, A.O., Luo, X., Mohan, M.L., Cohen, M.L., Chen, F., Kong, Q., Bartz, J., Singh, N. (2009). Abnormal brain iron homeostasis in human and animal prion disorders. *PLoS Pathog.*, 5, e1000336.
- Thomas, L.O., Boyoko, O.B., Anthony, D.C., & Burger, P.C. (1993). MR detection of brain iron. *Am J Neuroradiol*, 14(5), 1043-1048.
- Thorvaldsson, B., Hofer, S.M., Hassing, L.B., & Johansson, B. (2005). Cognitive change as conditional on age heterogeneity in onset of mortality-related processes and repeated testing effects. In S.M. Hoffer and D.F. Alwin (Eds.) *Handbook of cognitive Aging: Interdisciplinary Perspectives*, pp. 248ff. Sage Publications.

- Tingey, A.H. (1938). The iron content of the human brain –II. *J Ment Sci*, 84, 980-984.
- Todorich, B., Pasquini, J.M., Garcia, C.I., Paez,P.M., & Connor, J.R. (2009). Oligodendrocytes and myelination: The role of iron. *Glia*, 57, 467–478.
- Uehara, T., Tabuchi, M., & Mori, E. (1990). Risk factors for silent cerebral infarcts in subcortical white matter and basal ganglia. *Stroke*, 30, 378-382.
- Underwood, B.J. (1975). Individual differences as a crucible in theory construction. *American Psychologist*, 30(2), 128-34.
- Valenzuela, M.J. (2008). Brain reserve and the prevention of dementia. *Current Opinion in Psychiatry*, 21(3), 296-302.
- Vymazal, J., Brooks, R.A., Patronas, N., Hajek, M., Bulte, J.W.M., & Di Chiro, G. (1995a). Magnetic resonance imaging of brain iron in health and disease. *J Neurol Sci*, 134 (Suppl.), 19-26.
- Vymazal, J., Hajek, M., Patronas, N., Fiedd, J.N., Butte, J.W.M., Baurngarner, C., Tran, V., & Brooks, R.A. (1995b). The quantitative relation between T1-weighted and T2-weighted MRI of normal gray matter and iron concentration. *J Magn Reson Imaging*, 5(5), 554-560.
- Wagner, M., Jurcoane, A., Volz, S., Magerkurth, J., Zanella, F.E., Neumann-Haefelin, T., Deichmann, R., Singer, O.C., & Hattingen, E. (2012). Age-related changes of cerebral autoregulation: New insights with quantitative T2'-mapping and pulsed arterial spin-labeling MR imaging. *AJNR*, 33, 2081-87.
- Walters, G.D. (2011). Dementia: Continuum or distinct entity. *Psychol Aging*, 25(3), 534-544.
- Walsh, A.J., Belvins, G., Lebel, R.M., Seres, P., Emery, D.J., & Wilman, A.H. (2014). Longitudinal MR imaging of iron in multiple sclerosis: An imaging marker of disease.

- Radiology*, 270(1), 186-96.
- Winship, C. & Morgan, S.L. (1999). The estimation of causal effects from observational data. *Annu. Rev. Sociol.*, 25, 659-706.
- Xiang, Z., Nesterov, E.E., Skoch, J., Lin, T., Hyman, B.T., Swager, T.M., Bacskai, B.J., & Reeves, S.A. (2005). Detection of myelination using a novel histological probe. *J Histochem Cytochem*, 53, 1511-1516.
- Xu, X., Wang, Q., & Zhang, M. (2008). Age, gender, and hemispheric differences in iron deposition in the human brain : An *in vivo* MRI study. *NeuroImage*, 40, 35-42.
- Yates, P.A., Sirisiri, R., Villemagne, V.L., Farguharson, S., Masters, C.L., Rowe, C.C., & AIBL Research Group. (2011). Cerebral microhemorrhage and brain β -amyloid in aging and Alzheimer disease. *Neurology*, 77(1), 48-54.
- Zecca, L., Youdim, M., Riederer, P., Connor, J., & Crichton, R. (2004). Iron, brain ageing and neurodegenerative disorders. *Nat. Rev. Neuroscience.*, 5, 863-873.
- Zhang, S., Wang, J., Song, N., Xie, J., & Jiang, H. (2009). Up-regulation of divalent metal transporter 1 is involved in 1-methyl-4-phenylpyridinium (MPP⁺)-induced apoptosis in MES23.5 cells. *Neurobiol Aging*, 30, 1466-1476.

ABSTRACT**ACCUMULATION OF SUBCORTICAL IRON AS A MODIFIER OF VOLUMETRIC AND COGNITIVE DECLINE IN HEALTHY AGING: TWO LONGITUDINAL STUDIES**

by

ANA M. DAUGHERTY**August 2014****Advisor:** Dr. Naftali Raz**Major:** Psychology**Degree:** Doctor of Philosophy

Accumulation of non-heme iron in the brain has been theorized as a cellular mechanism underlying global neural and cognitive decline in normal aging and neurodegenerative disease. Relatively few studies of brain iron in normal aging exist and extant studies are almost exclusively cross-sectional. Here, I estimated iron content via T2* and measured volumes in several brain regions in two independent samples of healthy adults. The first sample (N = 89) was measured twice with a two-year delay and the second sample (N = 32) was assessed four times over a span of 7 years. Latent models estimated change in iron and volume, and the effects of cardiovascular risk factors as modifiers of change trajectories. Iron significantly increased (T2* decreased) over time in the basal ganglia, but not in the hippocampus. Accumulation of iron accounted for shrinkage in the striatum. Elevated metabolic syndrome risk indicators were associated with greater iron at baseline, which accounted for individual differences in shrinkage. Increase in caudate iron content was associated directly with lesser improvement in virtual Morris water maze navigation, and indirectly via shrinkage with lesser improvement in verbal working memory. This study presents the first longitudinal evidence in support of iron as a

biomarker of age-related decline in regional volume and cognition.

AUTOBIOGRAPHICAL STATEMENT

EDUCATION

INSTITUTION AND LOCATION	DEGREE	YEAR	FIELD OF STUDY
Westmont College, Santa Barbara, CA	B.S.	2007	Neuroscience, Experimental Psychology
Wayne State University, Detroit, MI	M.A.	2011	Psychology, Behav. Cog. Neuroscience
Wayne State University, Detroit, MI	Ph.D.	Current	Psychology, Behav. Cog. Neuroscience

SELECTED AWARDS AND HONORS

1. Institute of Gerontology Graduate Student Presenter, 1st place, Jan 2014
2. Graduate Psychology Poster Award, 1st place, Nov. 2013
3. Elizabeth Olson Memorial Paper Award, May 2013
4. Julie A. Thomas Memorial Research Award, Mar. 2013; Mar. 2014
5. Steven A. Lewis Memorial Research Award, Apr. 2012
6. IOG Student Presenter Travel Award, Feb. 2010; Feb. 2011; Oct. 2011; Oct. 2012; Nov. 2013; Feb. 2014
7. Dean of Students Presenter Travel Award, Feb. 2010, Feb. 2011

SELECTED PUBLICATIONS

- Daugherty, A.M., Yuan, P., Dahle, C.L., Bender, A.R., Yang, Y., Raz, N. 2014. Path complexity in virtual water maze navigation: Differential associations with age, sex, and regional brain volume. *Cerebral Cortex*. [Epub ahead of print].
- Adamo, D.E., Daugherty, A.M., Raz, N. Brain iron content and grasp force-matching ability in older women. *Brain Imaging and Behavior*. [Epub ahead of print].
- Yuan, P., Daugherty, A.M., & Raz, N. (2013). Turning bias in virtual navigation: age-related differences and neuroanatomical correlates. *Biological Psychology*, 96C, 8-19. doi: 10.1016/j.biopsycho.2013.10.009
- Bender, A.R., Daugherty, A.M., Raz, N. (2013). Vascular risk moderates associations between hippocampal subfield volumes and memory. *Journal of Cognitive Neuroscience*, 25(1), 1851-1862. doi: 10.1162/jcon_a_00435.
- Daugherty, A. & Raz, N. (2013). Age-related differences in iron content of subcortical nuclei observed in vivo: A meta-analysis. *NeuroImage*, 70, 113-121. doi: 10.1016/j.neuroimage.2012.12.040.
- Rodrigue, K.M., Daugherty, A.M., Haacke, E.M. & Raz, N. (2012). The role of hippocampal iron content and hippocampal volume in age-related differences in memory. *Cerebral Cortex*, 23(7), 1533-41. doi: 10.1093/cercor/bhs139.